DYNAMIC RESPONSE OF INTERVERTEBRAL JOINTS OF A SEATED FARM MACHINE OPERATOR IN THE RANGE 5-50 HZ.

Dissertation for the Degree of Ph. D.
MICHIGAN STATE UNIVERSITY
OSCAR ANTONIO BRAUNBECK
1976

This is to certify that the

thesis entitled

Dynamic Response of Intervertebral Joints of a Seated Farm Machine Operator in the Range 5 - 50 Hz.

presented by

Oscar Antonio Braunbeck

has been accepted towards fulfillment
of the requirements for

Ph. D. degree in Agricultural Engineering

Robert H. Wilkinson

Major professor

Date JAN. 27 1976

O-7639

ABSTRACT

ABSTRACT

Dynamic Response of Intervertebral Joints of a Seated Farm Machine Operator in the Range 5 - 50 Hz.

by

Oscar Antonio Braunbeck

There are a number of reports that consider vibrations as a cause of low back pain in subjects operating tractors, trucks, or buses over long periods of time. No objective explanation exists which is able to describe even qualitatively the mechanism by which seat vibrations generate spinal problems. An hypothesis is proposed which suggests that if intervertebral joint deformations present distinct levels at frequencies encountered in the seat of farm machinery, they will create a fatigue type loading of the intervertebral joint sufficient to induce pain sensations.

A lumped parameter dynamic model of the upper torso and head is proposed, whose main objective is to predict lumbar intervertebral joint deformations. The governing differential equations of motion are written for a linear system exposed to sinusoidal small amplitude displacement excitation in the vertical direction through the pelvis. A

Dynamic Response of

particular solution is found for the system of 58 second order differential equations that provides an equal number of complex amplitudes of motion, corresponding to each one of the degrees of freedom in the system. The rheological behavior of deformable components of the structure is modeled by means of Kelvin viscoelastic elements. The stiffness and damping coefficients for the axial mode of oscillation are derived from impedance data taken from isolated vertebral units.

The model is validated by computing seat to head transmissibility as well as driving point impedance coefficients over the frequency range 5-50 Hz. The transmissibility and impedance curves corresponding to the model closely resemble the experimental curves even though the values differ somewhat.

The magnitude of axial and shear deformations of intervertebral joints are significantly affected by the frequency of excitation and the characteristics of the seat or cab suspension used.

Axial deformations can be as high as 20% of the amplitude of base oscillation for an operator sitting on a bare vibrating table. The use of a spring-damper-mass suspension results in joint deformations about 1/4 to 1/5 those corresponding to a seat with no suspension.

Cab suspension results in smaller joint deformations than seat suspension for frequencies over 10 Hz. Between 5 and 10 Hz the seat suspension gives lower deformations.

Joint deformations increase with suspension damping. The best protection is offered by low damping ratios (ζ=0.1) provided the large amplitude of motion taking place at frequencies close to the seat natural frequency can be controlled.

Approved: Robert H. Wilkinson
Major Professor

Approved: D. R. Heldman
Department Chairman

Joint deformations increase with suspension damping. The best protection is offered by low damping ratios (ζ=0.1) provided the large amplitude of motion taking place at frequencies close to the seat natural frequency can be controlled.

Approved: Robert H. Whittemore
Major Professor

Approved: D. R. Heldman
Department Chairman

DYNAMIC RESPONSE OF INTERVERTEBRAL JOINTS OF A SEATED FARM MACHINE OPERATOR IN THE RANGE 5 - 50 HZ.

By

Oscar Antonio Braunbeck

A DISSERTATION

Submitted to
Michigan State University
in partial fulfillment of the requirements
for the degree of

DOCTOR OF PHILOSOPHY

Department of Agricultural Engineering

1976

ACKNOWLEDGMENTS

The author wishes to express a deep appreciation to Dr. Robert H. Wilkinson (Agricultural Engineering) for his guidance, enthusiastic support, and friendship during the course of the program.

Appreciation is extended to Dr. L. Segerlind (Agricultural Engineering), Dr. W. Sharpe (Metalurgy, Mechanics and Material Science), and Dr. L. Wolterink (Physiology) for their time and helpful suggestions as members of the guidance committee.

Dr. L. Kazarian (Aero Medical Research Laboratory, Dayton, Ohio) is acknowledged for his permission to use the impedance data collected from isolated vertebral units.

Many thanks are due to Mss Sonia Gonzalez for her assistance in preparing paper tape and cards for data prcessing, as well as typing the draft and original copies of this dissertation.

TABLE OF CONTENTS

LIST OF TABLES

LIST OF FIGURES

LIST OF SYMBOLS

$\{A\}$: Vector of complex amplitudes for all degrees of freedom in the system (cm)

A_e : Effective cross sectional area of intervertebral disc, (cm^2)

A_b : Amplitude of base oscillation (real), (cm)

A_j : Complex amplitude of oscillation of the jth. degree of freedom

A_j^r : Real part of complex amplitude

A_j^i : Imaginary part of complex amplitude

A_s : Complex amplitude of sacrum oscillation

$\{B_j\}$: Vector of damping and stiffness coefficients at the jth iteration

BS : Seat-base relative motion

C_c : Damping coefficient of chair suspension (dyn.sec/cm)

E : Young's modulus of elasticity of an intervertebral joint (dyn/cm^2)

F_s : Amplitude of sinusoidal forcing function (dyn)

F_s^r : Real part of complex force amplitude

F_s^i : Imaginary part of complex force amplitude

G : Shear modulus of elasticity of an intervertebral joint (dyn/cm^2)

G_1 : Age group being less than 30 years

G_2 : Age group being between 30 and 50 years

G_3 : Age group being over 50 years

I_g : Mass moment of inertia of a vertebra about its center of gravity (dyn. sec^2/cm)

I_{li} : Mass moment of inertia of ith lumbar vertebra about its center of gravity

I_{ti} : Mass moment of inertia of ith thoracic vertebra about its center of gravity

K_c : Stiffness of chair suspension spring (dyn/cm)

K_s : Shear stiffness of intervertebral joint (dyn/cm)

K_a : Axial stiffness of intervertebral joint (dyn/cm)

K_b : Bending stiffness of intervertebral joint (dyn.cm/rad)

M : Mechanical mobility (cm/dyn.sec)
M^r: Real part of mechanical mobility
M^i: Imaginary part of mechanical mobility

M'_j : Mechanical mobility of jth Kelvin element in parallel with mass m_j

M_c : Mass of chair (gm)

$[R]$: Rotation matrix

$[R_t]$: Transformation matrix

SS : Sum of squares function for optimization of model parameters

T : Period of oscillation of pendulum (sec)

T_r : Seat to head transmissibility

V : Velocity (cm/sec)

W : Weight of oscillating body (dyn)

$[W]$: Weighting matrix

$[X]$: Sensitivity matrix

X1,Z1: Coordinates of vertebra superior end plate, X1=0

X2,Z2: Coordinates of inferior end plate, X2=0

Xi,Zi: Coordinates of inferior costo-vertebral joint

Xs,Zs: Coordinates of superior costo-vertebral joint

$\bar{X}_j$: Complex amplitude of oscillation of jth mass along x-axis.

Xt,Zt: Coordinates of transverse costo-vertebral joint

Y : Experimental value of mechanical impedance
Y^r: Real part of experimental impedance
Y^i: Imaginary part of experimental impedance

Z : Mechanical impedance (dyn.sec/cm)

$Z(\beta)$: Modeled mechanical impedance ($Z^r + i\, Z^i$)

Z_a : Mechanical impedance of posterior arch

Z_b : Mechanical impedance of anterior spine (discs plus vertebral bodies)

Z_c : Mechanical impedance of a viscous damper

Z_k : Mechanical impedance of a linear spring

Z_m : Mechanical impedance of a single mass

Z'_j : Mechanical impedance of jth Kelvin element

Z''_j : Mechanical impedance of jth Kelvin element in parallel with mass m_j

$\bar{Z}_{head}$: Complex amplitude of head vertical motion

Z_j : Complex amplitude of oscillation of jth mass along z - axis

c : Viscous damping coefficient (dyn.sec/cm)

$[c]$: Damping matrix

c_a Viscous damping coefficient posterior arch

c_d : Viscous damping coefficient intervertebral disc

c_1, c_2: Parameters for estimation of frequency dependent viscous damping coefficients

d_1, d_2: Principal diameters of rib elliptical cross section

$f(t)$: Time dependent forcing function (dyn)

fq : Frequency of oscillation in (Hz)

g : Acceleration of gravity, (980.44 cm/sec^2, E. Lansing)

k : Linear spring stiffness coefficient (dyn/cm)

k_s : Shape factor of disc cross section

$[k]$: Global stiffness matrix

$[k_e]$: Element stiffness matrix in global coordinates(x,z,δ)

$[k_l]$: Element stiffness matrix in local coordinates (u,w,δ)

k_1, k_2: Parameters for estimation of frequency dependent spring stiffness coefficients

l : Height of intervertebral disc (cm)

m : Mass (gm)

m_h : Lumped mass of head and neck (gm)

m_j : Mass of jth vertebra without surrounding tissues (gm)

m'_j : Mass of jth vertebra with surrounding tissues (gm)

m_{li} : Mass of ith lumbar vertebra with surrounding tissues

m_{sp} : Lumped mass of sacrum and pelvis

m_{ti} : Mass of ith thoracic vertebra with surrounding tissues

m_{ut} : Lumped mass of upper torso and upper limbs

$[m]$: Mass matrix

$q(t)$: Generalized coordinates to describe motion of vibrating system (cm)

$q_s(t)$: Coordinate describing vertical motion of sacrum

r : Distance from pivot point to center of gravity of oscillating body (cm)

s : Independent variable in Laplace domain

t : Time (sec)

(u,w,δ): Local coordinate system

(x,z,δ): Global coordinate system

$z_b(t)$: Vertical displacement of seat base (cm)

Δ : Complex amplitude for rotational mode of motion

θ_i : Angle made by longitudinal axis of a vertebra and vertical z - axis

$\bar{\theta}_i$: Angle made by the longitudinal axis of an intervertebral disc and the z axis

θ_{12} : Angle made by vertebra end plate and disc middle plane a-a

ψ_i : Phase angle of ith degree of freedom relative to pelvis or base motion (deg)

α : Level of statistical significance

β : Stands for either c or k in sensitivity matrix X

δ_i : Rotation of a vertebra about its c.g. in sagittal plane.

ω : Angular frequency (rad/sec)

I. INTRODUCTION

1.1 Definition of the Problem

This investigation was primarily motivated by reports of low back pains suffered by farmers. However, the range of applications is much wider than just for agricultural situations. Truck drivers and operators of heavy equipment also experience the same symptoms. Excessive intervertebral joint deformation, over long periods of time, is probably a cause of backaches in seated operators subjected to vibrations. The conditions under which these deformations occur are investigated so that corrective measures may be taken.

1.2 Evolution of the Human Environment

Humans have been exposed to vibrations for centuries but, as civilization has progressed, the range of vibrational frequencies and amplitudes has become more severe. During the last hundred and fifty years science has changed the human working environment more than in the thousands of years since agriculture was first developed. So it is wise to look at the possible consequences that environmental changes may have on the human being.

During the period of the industrial revolution, productivity was the main concern, and very little attention was paid to the effects of the high level of physical and psychological stress placed on the human being. A similar situation took

place in agriculture. Farm productivity increased with mechanization, but the farmer was subjected to higher levels of physical and mental stress.

Power equipment possibly would not have become a health hazard if farmers had continued farming about the same area, but spent less time in field operations. However, because of economic pressures, the number of working hours remained about the same or in many cases increased, (machines do not need to rest as do horses) and the cultivated area increased to raise the economic output.

1.3 Vibrations as a Cause of Backache

Due to his inherent flexibility and great ability to "adapt" man has, for the most part, been able to adjust to the changing situations. But the "cost" in comfort, physical and mental stress, and general health has often been high. Too often solutions to environmental problems are not considered important until a problem becomes so acute that a solution is absolutely required.

Occupational health problems associated with operation of farm equipment by a seated operator exposed to body vibration is a kind of problem for which there exists no quick, easy, and conclusive evidence of damage to human health. There is some epidemiological association between vibrations and lumbar spine disorders, but conclusive evidence is not available yet. Large intervertebral joint deformations appearing over prolonged periods of time may not be the only cause of low back pain. Nonetheless, the population at risk

is sufficiently large, Wasserman et al. (1974), and some of the associated complaints are sufficiently severe that an attempt must be made to reduce the vibration induced joint deformations at points where they are extreme, and to concurrently conduct studies seeking to explain the relationship existing between the spine disorder and the vibration.

Even though there is no information on what magnitude of disc deformation under sinusoidal excitation could be harmful the present model will indicate the frequency ranges most likely to present tolerance problems. This means that protective systems (seat or cab suspension) can be designed without complete knowledge of the tolerance levels, with assurance that whatever the tolerability, the protection system will offer maximum protection.

Improper lifting habits are frequently considered to be the main cause of back problems. The total bending and axial load applied to the human torso when lifting a heavy weight are undoutedly higher than loads resulting from low amplitude seat vibration. But, in a lifting situation there is additional assistance to the spine through elevation of the intra-abdominal pressure that transforms the thorax and abdomen into a semi-rigid-walled cylinder, Eie (1972). This partially counteracts the compression produced by the erector spinae muscles and tends to elongate and straighten the lumbar spine anteriorly. The high intra-abdominal pressure which occurs when lifting heavy weights explains why certain individuals

may expose their back to extremely heavy loads without damaging their spine. This type of assistance is not available to the spine in a long duration vibratory load situation.

1.4 Dynamic Model of the Spine for Agricultural Applications

Most of the models reported in the literature have been developed for automobile and aerospace applications, mainly for short duration high acceleration seat ejection or front collision phenomenon. Farm equipment operators are subjected to vibrations of lower accelerations but for much longer periods of time and in a frequency range where several components of the body reach a resonant stage.

The vibration reaching the operator through the seat is mostly sinusoidal in nature, originating at engine, tires, transmission or some other moving component having rotary or reciprocating motion. Some terrain-induced random vibrations will also reach the operator with occasional transient peaks, mainly when crossing deep furrows where the seat suspension may bottom out.

The vertebral column of a seated tractor driver is frequently overstressed as the operator turns around to look at the machine pulled by the tractor. Yet some controls must be adjusted during tractor operation as a function of crop condition. This adds an extra load on the spine while it is simultaneously twisted and receiving a vibrational input through the pelvis.

1.5 Complexity of a Model of the Human Torso

The development of a mathematical dynamic model of the human torso involves problems such as complexity of the system; strong limitations for testing system components under normal operating conditions (in vivo) to collect data to validate the model; and materials as well as loads with poorly understood behavior.

Because of the structural complexity of the vertebral column and the difficulty of conducting experiments "in vivo", the dynamic behavior of the spine must be investigated through some kind of physical or mathematical model. The model can then be successively adjusted until it predicts the dynamic response of the human body with sufficient accuracy.

By working with a mathematical model rather than with a physical model it is easier to make modifications such as changes of size, shape or rheological properties of the connective tissue for any of the anatomical components of the system. A physical model would require the construction of new components, every time a dimension, shape or material has to be changed.

Dynamic modeling of most engineering structures is normally done for well understood material and structural members having known dimensions. The human body is very complex, mainly because there are large variabilities of dimensions from person to person, because connective tissues present non-linear viscoelastic behavior and because muscles do not

behave as passive structural components.

Measurements made on cadavers are hardly sufficient to permit production of statistically valid geometrical data of the structural components involved in a lumped parameter model. For some components approximations must be made through standard geometrical figures in order to be able to calculate the parameters required for a dynamic analysis. For instance, the geometry of a rib can be approximated by an elliptical cross section with variable ratios of the diameters, d_1/d_2, over the length of the rib.

Body materials tend to change with age more than engineering material do. The ideal situation would be to model the human body using data (rheological and geometrical properties) taken in vivo from young subjects of different ages, but in practice the properties are mainly measured from older cadaver materials. This is a limitation since cadavers have dynamic properties which are often different from the in vivo case. More accurate results will become available for modeling as new transducers are developed which are capable of taking measurements in vivo.

The loading conditions are also quite different from other engineering cases. This difference is mainly due to the existance of muscle forces which load the body structure following a stimulus mechanism not sufficiently understood to be properly modeled. But, for steady state low-amplitude vibratory excitation, the back muscles can be thought as exerting a constant axial force that contributes a great deal

to the stability of the spine. This assumption applies to a subject sitting erect, and not performing any tasks that could alter the symmetry of loads with respect to the sagittal plane. This is in fact the situation for most of the time of exposure to vibrations of a tractor driver. The thoracolumbar spine is capable of supporting very low compressive axial loads without muscle assistance.

1.6 Main Contributions Made by the Model

The number of approximations made when developing models of this kind will probably lead to results significantly less accurate than those reached in dynamic engineering structures made out of better understood materials. In spite of these uncertainties, there are positive contributions, such as:

a) A better understanding is gained both of critically loaded areas of the body and of the most critical loading conditions.

b) The need for specific geometric as well as rheological properties becomes evident.

c) Interdisciplinary interaction becomes more effective as the contributions made by the modeling work become known in other related fields.

1.7 Objectives

The steps followed in studying the spine problem presented through this chapter can be summarized in seven basic objectives:

1. Study existing reports on back problems of tractor

vibration could be considered to contribute significantly to the back pain.

2. Propose an hypothesis on how low amplitude vibrations acting vertically on the pelvis of a seated subject can adversely affect the lumbar spine.
3. Find the most realistic way to predict the dynamic response of the spine to sinusoidal input through the sacrum. This implies the simplification of a complex system to a model that can be mathematically implemented and solved.
4. Review existing data on the geometrical and rheological properties of the system in order to reduce experimental work to a minimum.
5. Verify the proposed model with existing data on overall dynamic response of the human torso for a body in sitting posture.
6. Draw conclusions and give recommendations concerning the most critical vibrational inputs to be minimized by a properly designed protective system.
7. Give recommendations on additional data required to reach more accurate results using the proposed model.

II. REVIEW OF LITERATURE

2.1 Surveys on Spinal Problems

The existing reports on back problems in subjects exposed to seat vibrations justifies the development of a model able to identify the vibratory conditions most adversely affecting the spine. The reports summarized in this section lead to the conclusion that vertical seat vibration is to some degree responsible for certain reported back problems.

Paulson (1949) observed some of the distressing symptoms of tractor driving during a period of several years of rural medical practice. The complaints ranged from neck stiffness and extremity pain, to digestive upsets, frequent stools, heartburn, urinary frequency and dizziness; but the most common complaint was lower backache.

Rosegger and Rosegger (1960) examined 371 tractor drivers to assess the correlation existing between vibrations, shocks, stomach troubles, and degenerative deformations of the thoracic and lumbar spine. They concluded: "Adolescent kyphosis can be caused not only by lifting or carrying heavy loads or prolonged work in a bent position during puberty and adolescence, but that it is also promoted by shocks and vibrations which act as microtrauma upon the intervertebral discs while the body is hold in a faulty posture. The degenerative spine

deformations increase proportionately with the length of service as tractor drivers".

Baker and Wilkinson (1974) conducted an occupational health survey on 851 farmers. The study showed that one of every 5 Michigan farmers suffers chronic back pain. One of every 12 farmers had to make an adjustement in his farming activities due to back or knee problems. Improper lifting habits and exposure to machinery vibrations are suggested by the authors as the factors most likely to be responsible for the backache.

There are some types of dynamic loads acting on the spine with sufficient frequency and time of exposure to be considered a kind of vibratory condition. Fusco et al.(1963) examined sixty workers employed in the sheet metal stamping industry. In 60% of the cases X-rays showed signs of lumbo-sacral arthrosis. The vibrations are transmitted to the operator through the legs and arms. The dynamic load is not sinusoidal but periodic with a frequency of about 1 stroke per second.

Long time exposure to vibration of young subjects will very likely affect bone shape and structural characteristics. Prives (1960) has investigated the influence of work and sports on the skeleton of 3000 growing and scenecent organisms, over a period of 10 years. Significant variations of bone shape and structure were found for certain occupations and sports.

Some other effects of vibrations have been investigated

that could be due to excessive motion of nerves in the spinal cord. Hornick (1961) studied the effect of low frequency vertical vibration (1 to 7 Hz) on male subjects at several intensities (.15 to .35 g). The subjects were seated on a rigid chair upon a shake table. Tracking performance was significantly ($\alpha<.001$) affected by vibration but there was no relationship to either the intensity or frequency of vibration. Reaction time was not impaired by any frequency or intensity until after the vibration ceased.

Several types of morbidity patterns related to whole-body vibration were investigated by Gruber and Ziperman (1974). The information was collected from 1448 interstate bus drivers, and included the results of periodic physical examinations. The results of the statistical analysis indicate that whole-body vibration must be included in the etiology of back disorders.

The basic bus vibrations are in the range 0-15 Hz, with a mean acceleration of 0.05 g. A rough riding bus can reach a mean acceleration of 0.1 g., Clevenson and Leatherwood (1973). Equivalent information is not available for farm machinery but it is reasonable to expect figures significantly higher than those reported for buses.

Most of the work done in trying to identify etiological factors related to various disorders of the spine are survey type research. This approach has provided sufficient evidence to support the hypothesis of existence of vibration related spinal problems. Experimental as well as modeling

work are the next stage in the process of explaining the mechanism relating vibrations to low back pain.

2.2 Hypothesis on Low Back Pain

There is a list of possible causes for low back pain, but the tendency among orthopedic and neurological surgeons is to attribute low back pain to abnormalities in the lumbar intervertebral discs. Some clinical observations suggest that the pain may originate within the disc, but anatomical studies have failed to demonstrate the presence of nerve fibers within the annulus or nucleus pulposus. This seems to indicate that pain must originate in some of the neighboring elements interacting with the discs, namely vertebral bodies, posterior arch, and ligaments. All of them contain nerve fibers able to sense pain, Brown et al. (1957).

The oscillatory relative motion between vertebrae creates a fatigue type loading on the annulus fibrosus of the intervertebral disc, the cartilages of the articular facets, and the ligaments linking both vertebrae, which may be responsible for some tissue irritation that creates pain sensations. The axial motion of vertebrae is the main vibrational mode of the lumbar spine for a seated subject under vertical base motion. Due to the curvature of the spine, the vertical motion of the sacrum will also generate rotational as well as tangential (shear) deformations of the intervertebral joints in the sagittal plane. Relative motion between vertebrae is considerably reduced above the 10th. thoracic vertebra. The ribcage increases the stiffness of the thoracic

spine. Therefore the larger deformations in the lumbar spine together with the high incidence of complaints in this region of the spine indicates that some relationship must exist between backache and intervertebral joint deformations.

The sinusoidal compressive force applied to an intervertebral disc simultaneously subjected to a constant compressive force resulting from body weight creates a pressure gradient between the disc and the vertebral bodies enclosing it. According to the results of Brown et al. (1957), 1.0 to 2.5 cm^3 of volume losses occur on the lumbar intervertebral disc under axial (quasi-static) compressive load. It is suggested by the authors that the transference of mass from the nucleus of the disc across the cartilagenous plates results in a less uniform stress distribution over the annulus fibrosus and cartilaginous plates. A reduction of hydrostatic pressure inside the disc means that a larger share of the axial load must be carried by the annulus fibrosus. A similar phenomenon may take place when the intervertebral disc is subjected to sinusoidal compressive loads superimposed to a constant axial load.

Frequency and amplitude of motion as well as time of exposure to vibrations are probably the main parameters to be studied concerning spine problems. The combination of a frequency with corresponding minimum values of amplitude and time of exposure at which low back pain develops can be considered as a "failure" of the spine subjected to cyclic stresses. Such fatigue failure will not occur if the exposure

time is short enough to allow repair by healing. The intervertebral discs, because of lack of reparatory power, may be particularly susceptible to this type of failure, Kraus and Farfan (1972).

2.3 Existing Lumped Parameter Models of the Human Torso

Some of the lumped parameter models most closely related to the one developed in this project are summarized in this section. The limitations of these models to predict the response of a seated subject to sinusoidal seat excitation are pointed out in each case.

The lumped parameter model developed by Orne and King Liu (1971) is capable of predicting the displacements of individual vertebra subjected to transient loading conditions. The behavior of the discs under axial compression is modeled by a three-parameter linear viscoelastic solid. The behavior of this model under compressive load closely resembles experimental creep and relaxation curves. However, according to the analysis of the impedance data reported by Kazarian (1972), the same model does not provide satisfactory results for sinusoidal excitation over the frequency range 5-50 Hz.

The model presented by Orne and King Liu, like some others, considers the effect of the upper torso on the spine by eccentrically, but rigidly attaching a mass (2050.0 gm) to each vertebra. The magnitudes and moments of inertia of these masses were measured by Liu and Wickstrom (1973). It was felt that under sinusoidal excitation the model would

be more realistic if a smaller mass, corresponding to the tissues more closely attached to the spine, is considered as being rigidly attached to each vertebra. The remaining mass of the upper torso must be attached to the spine through some kind of deformable elements that would allow for the relative motion existing between the ribcage and the spine.

Prasad and King (1974) developed a lumped parameter model of the spine including Kelvin viscoelastic elements for the three modes of motion in the sagittal plane; this is axial, shear, and bending (rotational) motions. The stiffness and damping coefficients of the Kelvin element are considered to be constant. The behavior of the model is satisfactory for transient type loads, but, according to the results of the modeling work done using the impedance data reported by Kazarian (1972), Kelvin viscoelastic elements with constant damping and stiffness coefficients do not give satisfactory results for axial sinusoidal excitation. The upper torso is modeled in a similar way to Orne and King Liu (1971). This model considers transmission of load through the articular facets, which is a major new feature when compared to other models that include only the intervertebral disc.

Muksian (1970) proposes a lumped parameter model including all the joints of the vertebral column, head, pelvis, ribs, shoulders, viscera of the upper torso, and the action of corresponding muscles. The proposed system with between

65 to 70 separate masses is finally reduced to only seven masses due to the complexity of the original system. Individual vertebrae are not considered as separate masses in the final model consequently it does not provide any information on deformation of intervertebral joints.

Roberts and Chen (1970) developed an elastostatic finite element of the human thoracic skeleton. It includes sternum, ribs, costal cartilage and vertebral column. The soft tissues were neglected. This model is acceptable for static loads; it was used only as a first approximation toward the development of a dynamic model for the study of anterior chest trauma, occuring for example in automobile collisions.

2.4 Rheological Behavior of Deformable Components of the Human Trunk

Up to the present time the need of rheological data for human biostructural analysis has been such that almost any result able to shed some light into the field was welcomed. It is mainly because the required experimental material is difficult to obtain. Moreover, the apparatus used to measure rheological properties in most cases must be specially built for the particular shape of the speciment being tested.

It was felt that enough information is available in the literature to model the human spine and draw some important conclusion on its response to sinusoidal input through the pelvis and at the same time get a better understanding of what is the additional information more urgently needed

that would lead to more accurate results. A through literature search was done in order to keep the experimental work to a minimum. Christ and Dupuis (1963) investigated the motion of cervical and lumbar spine for a seated subject under sinusoidal seat vibration. The equipment used was an image intensifier and X-ray film equipment. The study was not extended to the thoracic spine because of the very indistinct pictures produced by this area. Only one frequency, 2 Hz, was used for the experiment. No data is reported on deformation of intervertebral discs. Probably the definition of the X-ray film was not satisfactory for such measurements. Bulk displacements of the spine and stomach are reported.

The model under study requires stiffness and damping coefficients for the Kelvin elements used to predict the rheological behavior of intervertebral joints, neck, and costo-vertebral joints. The three principal structural connections between adjacent vertebrae, namely the disc, plus the posterior facets, plus the interconnecting ligaments will be refered to as the intervertebral joints.

Most of the required information is available in the reports described in the following paragraphs. Due to the wide ranges of variation given by some authors for some of the parameters, more than one source will be cited whenever possible so more average figures can be used. Most of the rheological data available is focused on the axial behavior of the intervertebral discs or the intervertebral joints.

The data finally adopted for the model are given in Chapter VI.

In those limited cases where there is a choice priority was given to data obtained under experimental conditions similar to the conditions of operation of the model; such as parameters measured under harmonic loading were given priority over those measured under transient or static loading conditions. Measurements made on complete intervertebral joints had priority over those taken separately for discs or posterior arch. Data taken from fresh cadaver material had priority over embalmed cadaver materials. Data measured from cadavers being between 30 and 50 years of age were chosen when possible.

Different components of the body trunk have different stiffness characteristics. Ribs, head, pelvis, and vertebrae are much stiffer than intercostal tissue or intervertebral discs, Crocker and Higgins (1966). For the purpose of this investigation head, vertebrae, and pelvis will be considered as rigid bodies. Andriacchi et al. (1974) found that although rigid bodies were used to model calcified portions of the ribs, vertebrae and sternum, the model predicts cage deformations in close agreement with those measured experimentally for static loading conditions.

The stiffness and damping coefficients involved in modeling the axial behavior of intervertebral joints are derived from the impedance data reported by Kazarian (1972) for isolated vertebral units. Details on these data are

described as needed in sections 4.1 and 6.4. The impedance measurements were taken from preloaded vertebral units, subjected to sinusoidal axial excitation; these test conditions make the data particularly suitable for the model being developed herein.

The rheological data for bending mode of oscillation of intervertebral joints in the sagittal plane is adopted from Markolf and Steidel (1970), who have measured stiffness and damping of the intervertebral discs under harmonic loading for the following modes of oscillation: lateral and sagittal bending, torsion, and tension-compression. The disc was fixed to a table by one end, and to a mass a the opposite end. The mass was allowed to move as a single degree of freedom system either in axial, bending, or torsional mode of oscillation.

The stiffness was calculated from the measured natural frequency of the single degreee of freedom system oscillating in free vibration. The damping factor was estimated from the rate of decay of the vibration trace. Even though there are no data to support the hypothesis that these coefficients are frequency dependent, an exponential equation will be adopted by analogy with the axial behavior as explained in section 6.4.2.

The measurements made by Markolf and Steidel were done with the posterior arch sawed off for the axial test. It was done under the assumption that the posterior facets and ligaments play no important role for the transmission of

vertical loads through the column. It may be the case for static loading, but under dynamic loading conditions the amount of damping present in the posterior arch may develop significant velocity dependent forces being transmited between vertebrae.

The damping data for bending oscillation is adopted from Prasad and King (1974).

Very little is known about the shear rheological behavior of intervertebral joints. An approximation done by Orne and King Liu (1971) using data reported by Evans and Lissner (1959) is used in section 6.4.3 to calculate the shear stiffness coefficients required for the model.

No data is reported on damping coefficients for shear mode of oscillation, so a range of values will be analyzed in an attempt to bracket the real value, and see how sensitive the structure is to this parameter.

The two dimensional model (sagittal plane) developed by Prasad and King (1974) includes Kelvin models for axial, shear and bending behavior of the intervertebral discs. The axial stiffness coefficients modified from Markolf and Steidel (1970) range from $29{,}000.00 \times 10^5$ dyn/cm to 14,000.00 dyn/cm from top to bottom of the thoracolumbar spine. These data are within the range swept by the frequency dependent stiffness coefficients derived from the impedance data reported by Kazarian (1972), but leaning toward the lower values. This is reasonable since Prasad and King assigned additional stiffness to the posterior arch in parallel with

the discs.

The axial damping coefficients used by Prasad and King for intervertebral discs range between 18.0×10^5 and 44.0×10^5 dyn.sec/cm, which is close to the lower values calculated using frequency dependent equations derived from impedance data. No damping was considered for the posterior arch.

The bending stiffness coefficients reported by Markolf and Steidel vary between $3,884.0 \times 10^5$ and $23,305.0 \times 10^5$ dyn.cm/rad. Prasad and King increased these values to $67,853.0 \times 10^5$ dyn.cm/rad. for the lumbar spine, and to $135,706.0 \times 10^5$ dyn.cm/rad for the thoracic spine. Prasad and King justified these stiffness increases by the fact that Markolf and Steidel's measurements were made with no preload. Moreover, the ribcage further increases the bending stiffness in the thoracic region of the spine. Although this reasoning is correct the stiffness increases are much too high.

Prasad and King considered the upper torso divided in slices cut by a horizontal planes passing through the intervertebral joints. Each slice was modeled as an excentric rigid mass attached to the corresponding vertebra. These excentric masses attached rigidly to a vertebra create much more severe dynamic loads on the intervertebral discs than those that would result from a model having some kind of deformable element linking the mass of the upper torso to the spine.

King and Vulcan (1971) measured the gradient of force-deformation curves under axial dynamic loading conditions. Two segments of the spine were tested. One segment consisted of half T11, T12, plus half L1. The second segment included half L1, L2, and half L3. The rate of loading used was approximately 9,000.0 Kg/sec. Each segment included two joints, so the stiffness of each joint is twice that reported for the segment.

Segment		Fresh	Embalmed
T-12,	aver. stiff. =	$37,162.0 \times 10^5$	$38,434.0 \times 10^5$ dyn/cm
L-2,	aver. stiff. =	$23,726.0 \times 10^5$	$28,962.0 \times 10^5$ dyn/cm

These values are 27.0% higher than those calculated for 50 Hz using the equations for frequency dependent axial stiffness coefficients. This is a result of compounding both, deformation as well as velocity dependent forces into a single stiffness coefficient.

In all cases there was no significant increase of stiffness from fresh to embalmed specimen conditions at T-12 level.

2.5 Geometrical Data of Components Involved in the Model

The geometrical data required for assemblage of the model presented in Chapter III involves dimensions of vertebrae and location of their center of gravity, curvature of the spine, and location of the center of gravity of the head-neck system.

Most of the dimensions of vertebrae required for the model could have been obtained in the literature from measurements

taken by Lanier (1939) Prasad and King (1974), Schultz and Galante (1970), and Roberts and Chen (1970). Since no data is available on vertebra mass moment of inertia about its center of gravity in the sagittal plane, measurements had to be taken from an embalmed spine. All dimensions needed were taken from a single cadaver.

The curvature of the spine adopted for the model corresponds to a subject seated in erect posture on a seat furnished with low back rest, Clark et al. (1963). Data reported by Kazarian (1972), Orne and King Liu (1971), and Schultz et al. (1973) were consulted to gather all the information required.

The curvature of the spine considerably affects the amount of load to be carried by the intervertebral discs. A proper restraint system would keep the spine in an erect position, which makes the posterior arch to share a larger percentage of the load. Ewing et al. (1972) found that anterior compression of the lumbar vertebral column can be reduced by restraining the shoulders and pelvis to the seat back in a moderate hyperextended position.

The spine configuration used in the present study approximately corresponds to average tractor driving conditions. Moreover, the adopted relative position between vertebra is close to that used to collect the impedance data involved in modeling the axial rheological behavior of the intervertebral joints. Other configurations would have different stiffness coefficients for the intervertebral

joints if their non-linear force-deformation behavior is taken into consideration. Therefore more data should be available on the rheological behavior of the joints before any studies can be conducted in relationship to dynamic responce and body posture.

2.6 Masses Involved in the Lumped Parameter Model

The weight distribution of components over the human torso, head and upper limbs has been reported by a number of authors, Dempster (1955), Damon et al. (1966), Ingalls (1931), Lowrance and Latimer (1967), Muksian and Nash (1974), and Payne (1970).

Since the spinal data used for the model was measured on a spine corresponding to a body weight of 85.0 kg, most of the component weights will be calculated using Dempster's data given as percentage of body weight.

III. THE MODEL

3.1 Mayor Aspects of the Modeling Process

Prediction of relative motion between vertebrae of a seated human being under sinusoidal base excitation can be done through mathematical formulation. The human torso can be considered as an engineering structure whose dynamic response is the integrated response of all the components of the structure. Even though the spine is the only element of interest for the present work, the remaining elements of the torso (head, thorax) are included in the model only because of their interaction with the spine.

There are five mayor aspects to the modeling of the vertebral column:

1. Reduction of the real torso to a simplified version that will be easier to formulate but having a dynamic response close to that of the original system
2. Study of the kinematic behavior of the moving parts of the torso
3. Study of the rheological behavior of the deformable elements in the system
4. Derivation of the governing differential equations of motion
5. Solution of the system of governing equations of motion

3.2 Simplified Model of the Human Torso

The real system shown in Figure 3.1 has been properly reduced to the lumped parameter model of Figure 3.2, which is suitable for mathematical formulation. The simplifications involved in the process of reducing the actual structure to a model form are based on a number of assumptions:

1. Only the torso, head and upper limbs are included in the model. The lower limbs rest on the floor and the seat surface without actually loading the spine.
2. Vertebrae are considered as rigid bodies. Deformations of the spine under load take place at the intervertebral joints. All components of the spine are deformable, but the stiffness of vertebrae is much higher than that of ligaments and cartilages forming the intervertebral joints. Bell et al. (1967) reported a median vertebral bone stiffness of 11.0×10^9 dyn/cm compared to about 2.0×10^9 dyn/cm for the intervertebral joint.
3. The forces developed at intervertebral joints are assumed to be linear functions of deformations. The rheological behavior of the joints is nonlinear, Brown et al. (1957), but for deformations sufficiently small the behavior closely follows the equation of a straight line tangent to the force-deformation curve.
4. No temperature effects are considered in the rheological equations. The range of variation of body temperature is very small.
5. Ribcage, internal organs of the thorax, upper limbs, and

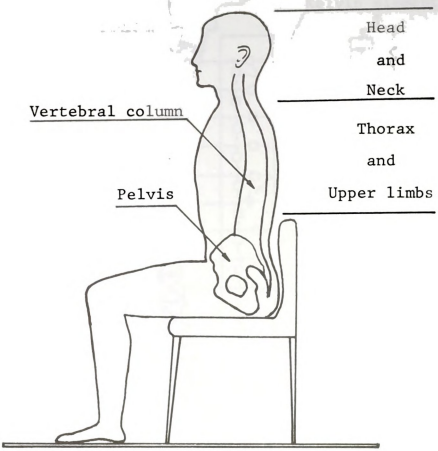

Figure 3.1. Components of a seated human body having significant dynamic interaction with the vertebral column.

head

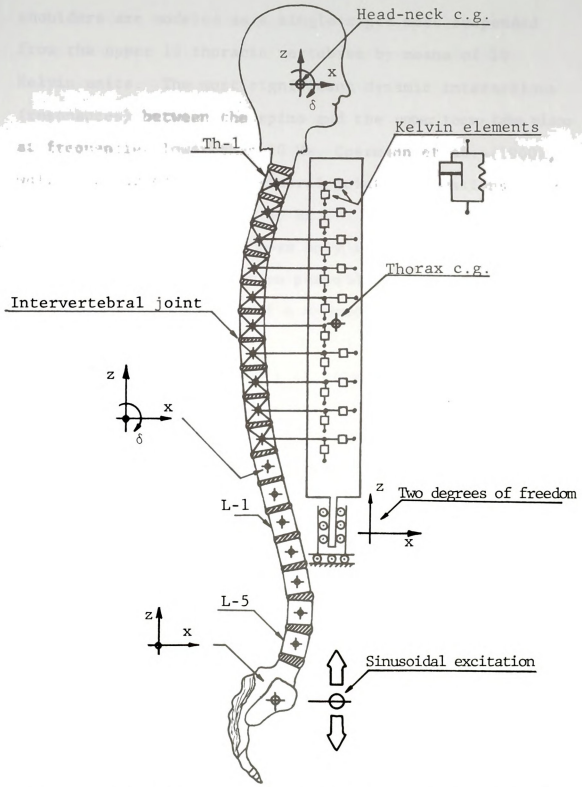

Figure 3.2 Simplified structure representing a seated human body.

shoulders are modeled as a single rigid mass suspended from the upper 10 thoracic vertebrae by means of 10 Kelvin units. The most significant dynamic interactions (resonances) between the spine and the upper torso take place at frequencies lower than 10 Hz, Coermann et al. (1960), while the largest intervertebral joint deformations take place between 30 and 40 Hz.

6. Vertebrae are assumed to move only in the sagittal plane. Forces acting in a direction perpendicular to the sagittal plane on both halves of a symmetric body will mutually cancel out.
7. Muscles enter the model only as passive components having dynamic interaction with the spine as a result of their mass and viscous behavior. Transient or random excitations that could trigger muscle activity other than the constant stabilizing force on the spine, are not included in the analysis. The response of the model attempts to predict intervertebral joint deformations for subjects under steady state sinusoidal excitation.
8. Head and neck are modeled as a single mass attached to the top end of the thoracic spine by means of three Kelvin elements representing the normal, shear and bending rheological behavior of the neck.
9. Since the abdominal organs are mostly resting on the pelvis they are considered as part of the pelvic mass. The dynamic response of the abdomen would mainly affect the values of driving point impedance that are used for validation

of the model. According to the results of Coermann et al. (1960) the motion of the abdominal wall presents a maximum at a frequency between 3 and 4 Hz for all subjects studied. The abdomen displacement curve levels off at about 7 Hz, with no other resonant conditions thereafter. It indicates that the abdominal mass is not responsible for any of the peculiarities presented by the impedance curve of a seated human body.

10. The impedance data used to derive the frequency dependent stiffness and damping coefficients were obtained from fresh cadavers. There is no doubt the properties of living tissues will deviate from those of the inert material. The magnitude of the deviation has yet to be investigated. The overall response of the model indicates that those deviations are not significant.
11. The intervertebral joint is modeled as a set of three massless Kelvin elements. The mass of the disc is divided in two parts which are considered as part of the two vertebral bodies enclosing the disc, see drawing in Table 6.2.

3.3 Kinematics of the Model Components

There are a number of deformable elements in the human torso that allow relative motion among components of the structure. The ones included in the model are: intervertebral joints, costo-vertebral joints and the neck.

The patterns of deformation assumed for an intervertebral joint along the disc axis (axial) as well as perpendicular

to it (shear) are shown in Figures 3.3 and 3.4. Pure bending deformation is assumed to occur when the relative motion between vertebrae takes place around the point of intersection, 0, of the longitudinal axis of the two vertebral bodies, see Figure 3.5. These simplified patterns of joint kinematic behavior are adopted under the assumption of small deformations.

The kinematic behavior of the intervertebral joint requires special techniques to handle geometric non-linearities when large relative displacements are allowed between vertebrae; for example in an hyperextended mode the articular facets on the spinal posterior arch will bottom out. It significantly changes the kinematic behavior of the intervertebral joint. Configuration and location of the articular facets and posterior arch are illustred in Appendix A.

The intervertebral joint flexibilities just introduced allow for each thoracic and lumbar vertebra to have three degrees of freedom in the sagittal plane that will be identified by coordinates x,z,δ as shown in Figure 3.6.

Sacrum and pelvis are included in the model as a single mass. Only two degrees of freedom, (x,z), are assigned to this mass. No significant pelvis rotations are expected in light of the following assumptions:

a) For subject seated erect the point where the seat interacts with the pelvis is almost on the same vertical line as the intervertebral joint L5 - S, so that no significant

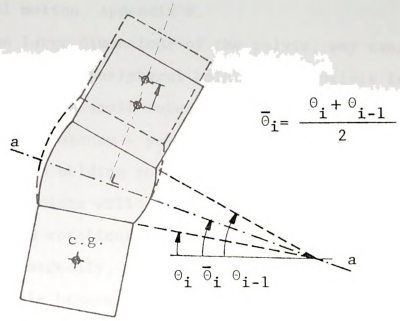

Figure 3.3. Axial deformation of intervertebral joint. The displacements between vertebrae is in a direction perpendicular to disc middle plane a - a.

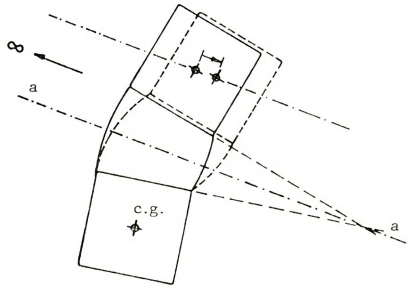

Figure 3.4. Shear deformation of intervertebral joint. The displacement between vertebrae is in a direction parallel to disc middle plane a - a.

moments are applied to the pelvis that could generate rotational motion, Appendix F.

b) Due to the large dimensions of the pelvis, any tangential displacement of a peripheral point of the pelvis is translated into a small rotation about the center of gravity of the sacrum - pelvis mass.

The ligaments holding together ribs and vertebrae at the costo-vertebral joints will allow significant relative displacements and rotations between a vertebra and a rib when loaded individually, Schultz et al. (1974). The ribcage as a whole behaves very much like a hollow truncated cone having mostly longitudinal and transversal displacements relative to the thoracic spine. Any rotational relative motion will be greatly inhibited by the line of costo-vertebral joints placed on the thoracic spine. Therefore, the mass of the upper torso, M_{ut}, is given only 2 degrees of freedom; with motion in horizontal and vertical directions.

The head has three degrees of freedom in the sagittal plane. None of them is inhibited to a point where its elimination from the model can be justified.

Each one of the degrees of freedom just described implies the existence of a corresponding coordinate if the motion of the structure is to be fully described. Therefore coordinates will be adopted according to the number of degrees of freedom assigned to each mass.

3.3.1 Systems of coordinates

A system of coordinates must be properly chosen before

writing the equations governing the motion of the structure. The resultant system of equations will have desirable characteristics depending on the chosen coordinates.

For the model under study, the motions of each vertebra and the head-neck lumped mass in the sagittal plane are completely described by three x, z, δ as shown in Figure 3.6. The z-axis is oriented vertically while the x-axis is oriented horizontally from the spine to the anterior part of the torso. The deflections are measured from a fixed point in space where the center of gravity of masses would be at rest if there were no excitation forces acting on the system.

A clockwise rotation δ of a mass about its center of gravity is assumed positive. The sacrum-pelvis and the upper torso masses are given only two degrees of freedom described by coordinates x and z. Coordinates u, w, δ shown in Figure 3.6 are auxiliary coordinates used to facilitate the derivation of the intervertebral joint stiffness matrix.

3.4 Rheological Behavior of Deformable Elements of the Model

The rheological behavior of all deformable elements in the system is modeled by means of Kelvin type viscoelastic elements as shown in Figure 3.2 to model the costo-vertebral joints. This decision was made in light of the results obtained from the modeling work done for the axial behavior of intervertebral joints, which is covered in chapter IV. The numerical values assigned to each spring and dashpot in the system are discussed in Chapter VI.

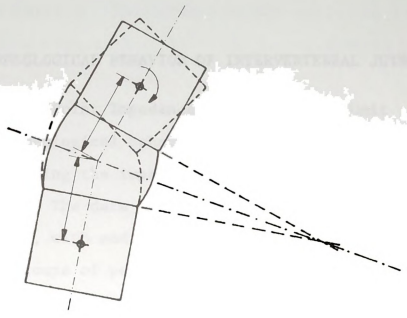

Figure 3.5. Bending deformation of an intervertebral joint.

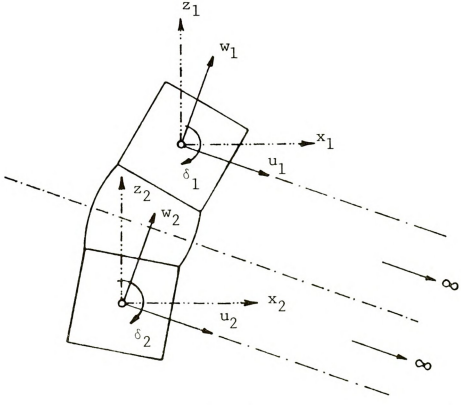

Figure 3.6. Local system of coordinates for calculation of element stiffness matrix.

IV. AXIAL RHEOLOGICAL BEHAVIOR OF INTERVERTEBRAL JOINTS

4.1 Driving Point Impedance of a Vertebral Unit

The axial rheological behavior of an intervertebral joint can be modeled using the impedance test results reported by Kazarian (1972). The data are available for the thoracic and lumbar spine, with and without the posterior arch, and for three age groups of people.

Some of the conditions under which Kazarian's tests were conducted are summarized in this section for application in Chapter IV. The thoracolumbar spine was divided in four units: T1-T6; T7-T12; L1-L3; and L4-Sacrum for impedance testing.

The vertebral units were tested in vertical position. The superior end of the unit was fixed to a loading head mounted on a ball joint designed to apply pure compression load on the unit. The lower end of the vertebral unit was mounted onto the shaker head, Figures 4.1 and 6.5. Each unit was tested at a preload of 21.7 Kg. This testing condition forced the intervertebral joints to a deformed configuration with higher values of stiffness and closer to the real situation.

Following the impedance test of a complete spinal unit, it was removed from the loading head, its posterior arch separated and the vertebral bodies with intact anterior and posterior ligaments were placed back into the loading jaws

for impedance testing. The later test was conducted to find out how the posterior arch contributes to the dynamic load carrying capacity of the spine.

4.2 Mechanical Impedance

Electrical circuit analysis techniques can be applied to complex mechanical systems. The mechanical impedance (or mobility) is a relationship between force and velocity represented by a differential equation in the time domain. By transforming this equation to the Laplace domain the computational work is considerably simplified since all the differential equations become algebraic. For the present investigation where harmonic excitation is the main interest and the answers sought can be obtained in the frequency domain, the Laplace variable, s, will be repleaced by $i\omega$, where i stands for the imaginary number $\sqrt{-1}$, and ω is the frequency of harmonic oscillation.

The impedance, Z, of the three basic elements (spring, dashpot, and mass), equations (4.1), are used to derive the impedance of the complete structure. The derivation of element impedances are given in Vernon (1967).

Mass	Damper	Spring	
$Z_m = \frac{F}{V} = ms$	$Z_d = c$	$Z_k = k/s$	(4.1)

where:

Z_m : Impedance of a mass ; F : Force

Z_d : Impedance of a damper ; V : Velocity

Z_k : Impedance of a spring ; m: Mass

c : Damping coefficient ; k: Stiffness coefficient

s : Laplace variable

It is convenient to use the concept of "mobility" at some points in the analysis of the structure. The mechanical mobility, M, is the reciprocal of the mechanical impedance.

$$M = 1/Z \qquad (4.2)$$

Whenever simple elements of the structure are in parallel, their velocities are the same, and the total force is the sum of the forces applied to each element. Since impedance is defined as the ratio: force/velocity, and the velocity is a common denominator to all parallel elements, the overall impedance of the parallel arrangement is simply the sum of the impedances of the individual elements.

For elements in series the same force is applied to all elements. Since "mobility" is defined as the ratio velocity/force, the denominator of all elements is equal, so the overall mobility of the arrangement is the sum of the mobilities of the components. The previous concepts are summarized by equations (4.3) and (4.4).

Elements in Parallel	Elements in Series
$Z = Z_1 + Z_2$	$Z = \dfrac{1}{1/Z_1 + 1/Z_2}$ (4.3)
$M = \dfrac{1}{1/M_1 + 1/M_2}$	$M = M_1 + M_2$ (4.4)

These simple concepts are sufficient to derive an equation

for the driving impedance of a vertebral unit composed of N masses (vertebral bodies) plus equal number of springs and dampers located between the masses. The viscoelastic elements representing the intervertebral joints were modeled as a pair spring-dashpot in parallel (Kelvin model). The damping and stiffness coefficients of the model are given as exponential functions of frequency in the range 5-50 Hz.

Models other than Kelvin, including three to five parameters were used in the modeling process in an attempt to predict the mechanical impedance of the vertebral unit using constant parameters. No satisfactory results were obtained from these models, so the Kelvin model with frequency dependent coefficients was finally adopted.

The driving point impedance of the vertebral unit shown in Figure 4.1 is calculated from the impedances and mobilities of the viscoelastic elements and masses in the system.

For the spring and dashpot in parallel the resultant impedance, Z'_j, is:

$$Z'_j = Z_c + Z_k = c + k/s \tag{4.5}$$

The impedance, Z''_j, of the jth. Kelvin element in parallel with mass m_j is given by equation (4.6). It must be converted to mobility, M''_j, so it can be added to the mobility of the superior part of the unit, $M_{(j-1)}$, with which it is in series, equation (4.7).

$$Z''_j = c + k/s + m_j s \tag{4.6}$$

The masses appear to be physically in series with the viscoelastic elements, but they must be considered as being in parallel for the impedance calculations using electrical analogy.

$$M''_j = \frac{1}{Z''_j} = \frac{1}{c + k/s + m_j s} \tag{4.7}$$

Substituting s by $i\omega$,

$$M''_j = \frac{1}{c - ik/\omega + i\omega m_j} = \frac{c}{D_0} + \frac{i(k/\omega - \omega m_j)}{D_0} \tag{4.8}$$

$$D_0 = c^2 + (\omega m_j - k/\omega)^2$$

The mobility at the bottom end plate of the jth vertebra, M_j, is the sum of the mobility (M_{j-1}) at the bottom end plate of the (jth-1) vertebra plus that corresponding to mass m_j in parallel with a Kelvin element.

$$M_j = M_{(j-1)} + M''_j = M^r_{(j-1)} + \frac{c}{D_0} + i\left[M^i_{(j-1)} + \frac{(k/\omega - \omega m_j)}{D_0}\right] \tag{4.9}$$

M^r, M^i : Real and imaginary parts of mechanical mobility respectively.

Equation (4.9) is sequentially applied from the first

movable vertebra at the top of the unit down to the last vertebra at the impedance head. The mobility of the first superior vertebra is null for being attached to a fix loading head. This known value is used in equation (4.9) to start the sequencial calculations from top to bottom of the unit.

The impedance of the whole vertebral unit, Z, is computed from the mobility, M_n, obtained for the nth vertebra (lowest) of the unit using equation (4.10).

$$Z = 1/M_n = M_n^r / |M_n|^2 - i\, M_n^i / |M_n|^2 \qquad (4.10)$$

4.3 Estimation of the Parameters of the Kelvin Model

The parameters c and k in the Kelvin model of the intervertebral joint can be calculated using the approach described by Beck and Arnold (1975). For the implementation of this procedure a matrix of sensitivity coefficient, $[X]$, must be calculated. Each sensitivity coefficient is the rate of change of the real or imaginary part of the mechanical impedance, Z^r and Z^i respectively, with respect to the damping coefficient c, or the stiffness coefficient k.

$$[X] = \begin{bmatrix} \frac{\partial Z^r}{\partial c} & \frac{\partial Z^r}{\partial k} \\ \frac{\partial Z^i}{\partial c} & \frac{\partial Z^i}{\partial k} \end{bmatrix} \qquad (4.11)$$

If β stands for either c or k, the two rows of the sensitivity matrix are given by equations, (4.12) and (4.13)

which were derived from equation (4.10).

$$\frac{\partial Z^r}{\partial \beta} = \frac{\frac{\partial M^r}{\partial \beta} |M|^2 - 2\left(\frac{\partial M^r}{\partial \beta} M^r + \frac{\partial M^i}{\partial \beta} M^i\right) M^r}{|M|^4} \qquad (4.12)$$

$$\frac{\partial Z^i}{\partial \beta} = \frac{\frac{\partial M^i}{\partial \beta} |M|^2 - 2\left(\frac{\partial M^r}{\partial \beta} M^r + \frac{\partial M^i}{\partial \beta} M^i\right) M^i}{|M|^2} \qquad (4.13)$$

$$\frac{\partial |M|^2}{\partial \beta} = \frac{\partial}{\partial \beta}\left[(M^r)^2 + (M^i)^2\right] = 2\left[M^r \frac{\partial M^r}{\partial \beta} + M^i \frac{\partial M^i}{\partial \beta}\right]$$

Where the partial derivatives of real and imaginary parts of the mobility can be obtained from equation (4.9), and are given by equations (4.14) to (4.17).

$$\frac{\partial M^r}{\partial c} = \frac{\partial M^r_{(j-1)}}{\partial c} + \frac{D_0 - 2c^2}{\omega D_0^2} \qquad (4.14)$$

$$\frac{\partial M^r}{\partial k} = \frac{\partial M^r_{(j-1)}}{\partial k} + \frac{2c(\omega m_j - k/\omega)}{D_0^2} \qquad (4.15)$$

$$\frac{\partial M^i}{\partial c} = \frac{\partial M^i_{(j-1)}}{\partial c} - \frac{(k/\omega - \omega m_j)\ 2c}{D_0^2} \qquad (4.16)$$

$$\frac{\partial M^i}{\partial k} = \frac{\partial M^i_{(j-1)}}{\partial k} + \frac{D_0/\omega + 2\ (\omega m_j - k/\omega)/\omega}{D_0^2} \qquad (4.17)$$

These derivatives are successively calculated for each intervertebral joint from the loading head down to the impedance head. The coefficients of the sensitivity matrix are obtained from equations (4.12) and (4.13) using the values of impedance and its derivatives calculated for the last vertebra of the unit.

The parameters in the model are optimized by minimizing the sum of squares function, SS, given by equation (4.18).

$$SS = \left[Y - Z(\beta) \right]^T W_h \left[Y - Z(\beta) \right] \qquad (4.18)$$

Y: Vector including real and imaginary parts of experimental impedance.

Z: Vector including real and imaginary parts of modeled impedance.

$$Y = \begin{Bmatrix} Y^r \\ Y^i \end{Bmatrix} \qquad Z(\beta) = \begin{Bmatrix} Z^r \\ Z^i \end{Bmatrix}$$

The weighting matrix, W_h, is taken as an identity matrix for the present work. The minimization of the sum squares is done by the linearization method (Gauss). From this minimization process the optimum values of the parameters c and k are obtained, after successive iterations using equations (4.19).

$$B_{(j+1)} = B_j + (X^T W_h^{-1} X)_j^{-1} X_j^T W_h^{-1} (Y - Z_0(\beta))_j \qquad (4.19)$$

$$B_j = \begin{Bmatrix} c_j \\ \\ k_j \end{Bmatrix} : \text{Vector of damping and stiffness coefficients after j iterations}$$

The sensitivity matrix X and modeled impedance Z (β) are re-evaluated after each iteration because they are function of the parameters c and k that change after each iteraction. The iterative procedure continues until the parameters change a negligible amount or until the sum of squares is sufficiently small.

4.4 Frequency Dependent Stiffness and Damping Coefficients

A damping coefficient and a stiffness coefficient are calculated for each data point consisting of a frequency, impedance modulus, and phase angle. The stiffness coefficients were found to increase exponentially with frequency while the damping coefficients decrease exponentially in the frequency range 5 to 50 Hz. Equations (4.20) and (4.21) give good approximations for the stiffness and damping coefficients. Coefficients k_1, k_2 and c_1, c_2 are listed in Table 6.5 for three age groups of people. They were approximated by the least square fit method.

$$c = c_1 \, (fq)^{c_2} \tag{4.20}$$

$$k = k_1 \, e^{k_2 \, fq} \tag{4.21}$$

4.5 Axial Dynamic Response of the Posterior Spinal Arch

The posterior vertebral arch contributes to the load carrying capacity of the spine. The portion of the load carried by the arch is dependent on the curvature of the spine in the sagittal plane. The load on the posterior arch varies with sitting posture. As the degree of hyperextension of a seated subject increases, so does the load on the posterior arch.

The impedance measurements made by Kazarian (1972) for vertebral units with and without posterior arch suggest the idea of modeling the intervertebral joint as a pair of viscoelastic elements (Kelvin) in parallel, Figure 4.2. The element, D, simulates the intervertebral disc; the second element, A, represents the posterior arch. The mechanical impedance of a vertebral unit is calculated sequentially from top to bottom of the unit adding impedances or mobilities according to convenience, as it was done in section 4.2 for a vertebral unit with single Kelvin elements between masses.

$$M_j = M_{(j-1)} + \frac{1}{Z_m + Z_a + Z_b} \qquad (4.22)$$

$$Z_m = ms \ : \text{ Impedance of mass representing vertebral body} \qquad (4.23)$$

$$Z_a = \frac{k_a}{s} + c_a \ : \text{ Impedance of posterior arch} \qquad (4.24)$$

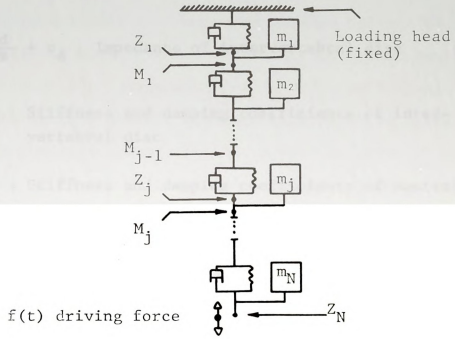

Figure 4.1. Spinal unit model for calculation of driving point impedance.

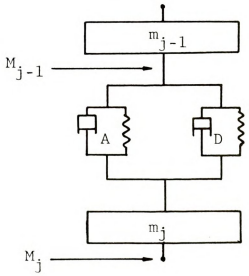

Figure 4.2. Intervertebral joint modeled as two Kelvin elements in parallel.

$$Z_b = \frac{k_d}{s} + c_d \quad : \text{Impedance of intervertebral disc} \qquad (4.25)$$

k_d, c_d : Stiffness and damping coefficients of intervertebral disc

k_a, c_a : Stiffness and damping coefficients of posterior arch

Substituting (4.23) to (4.25) in (4.22), and after introducing $s = i\omega$ for sinusoidal excitation, the real and imaginary parts of the mobility are:

$$M_j^r = M_{(j-1)}^r + \frac{(c_a + c_d)}{D_0} \qquad (4.26)$$

$$M_j^i = M_{(j-1)}^i + \frac{\left[\frac{(k_a + k_d)}{\omega} - m\omega\right]}{D_0} \qquad (4.27)$$

$$D = (c_a + c_d)^2 + \left[m\omega - \frac{(k_a + k_d)}{\omega}\right]^2 \qquad (4.28)$$

After the mobility for the last vertebra of the unit has been calculated the impedance of the unit is obtained using equation (4.10).

There are two damping coefficients, (c_a, c_d), and two stiffness coefficients (k_a, k_d) to be estimated in equations (4.26) and (4.27). The coefficients corresponding to the

Stiffness and damping coefficients of intervertebral disc

intervertebral disc (c_d, k_d) were already calculated using the impedance data "without arch" together with equations (4.9) and (4.10) corresponding to a model with single Kelvin elements between masses. Consequently only the stiffness and damping coefficients for the posterior arch, c_a and k_a, are left to be calculated from the impedance data "with arch".

In order to estimate the parameters c_a and k_a, the coefficients of the sensitivity matrix (4.11) are to be calculated from equations (4.12) and (4.13). Some of the partial derivatives in Equation (4.12) and (4.13) must be further expanded for implementation on digital computer. Equations (4.29) to (4.32) follow from (4.26) and (4.27).

$$\frac{\partial M_j^r}{\partial k_a} = \frac{\partial M_{(j-1)}^r}{\partial k_a} + 2\,(c_a + c_d)\frac{\left[m - \dfrac{(k_a + k_d)}{\omega^2}\right]}{|M_j|^4} \tag{4.29}$$

$$\frac{\partial M_j^r}{\partial c_a} = \frac{\partial M_{(j-1)}^r}{\partial c_a} + \frac{|M_j|^2 - 2\,(c_a + c_d)^2}{|M_j|^4} \tag{4.30}$$

$$\frac{\partial M^i}{\partial k_a} = \frac{\partial M^i_{(j-1)}}{\partial k_a} + \frac{|M_j|^2 - 2\ m\omega - \frac{(k_a + k_d)}{\omega}}{|M_j|^4} \qquad (4.31)$$

$$\frac{\partial M^i}{\partial c_a} = \frac{\partial M^i_{(j-1)}}{\partial c_a} + \frac{2(c_a + c_d)\ m\omega - \frac{(k_a + k_d)}{\omega}}{|M_j|^4} \qquad (4.32)$$

The sensitivity matrix is assembled with the results of equations (4.29) to (4.32). The optimization of parameters k_a and c_a is done by iteration using equation (4.19).

The stiffness coefficients obtained from the data "without arch" were in many cases greater than those corresponding to the data "with arch", what would apparently indicate that the posterior arch makes a negative or at least null contribution to the load carrying capacity of the spine. The phenomenon that actually took place is probably as follows: by removing the posterior arch and keeping a constant compression bias on the vertebral unit the disc moved to a larger deformation configuration able to carry the total load without the assistance of the posterior arch. Given the non-linear rheological behavior of the disc, the larger deformation imposed on the disc explains the larger values of stiffness obtained for the vertebral unit without arch.

The analysis in section 4.5 would probably lead to

correct results if impedance data were available for vertebral units without arch, but tested under the same levels of axial deformation used for the test with arch.

As a result of the previous findings, intervertebral disc and posterior arch were considered a single unit called "intervertebral joint". A single Kelvin element was used to model the joint, with coefficients c and k obtained from data with arch.

V. DYNAMIC RESPONSE OF THE LUMPED PARAMETER MODEL

5.1 Governing Differential Equations of Motion

The system of second order differential equations governing the motion of an N-degree of freedom system with viscous damping is as given by equation (5.1), Meirovitch (1967).

$$[m]\left\{\ddot{q}(t)\right\} + [c]\left\{\dot{q}(t)\right\} + [k]\left\{q(t)\right\} = \left\{f(t)\right\} \quad (5.1)$$

Where the mass matrix $[m]$, stiffness matrix $[k]$, and damping matrix $[c]$ were calculated using the procedure described in the three following sections. The displacement function $q(t)$ and the forcing function $f(t)$ are discussed in section 5.2.

Each equation (row) of the system (5.1) can be derived by writing the equation of dynamic equilibrium, Newton's 2nd. law, for each degree of freedom of each mass in the system. The result will be a system of equations resembling that shown as an example in Appendix B for the motion of a vertebra in x - direction. A less involved procedure would probably result from the application of Lagrange's equations. But, due to the large number of degrees of freedom in the system, a matrix approach was used that provides the equations of motion for the discrete system by properly choosing a coordinate system and applying some of the well established

techniques of structural analysis to derive the stiffness and damping matrices. This approach permits handling of the equations in a more compact and systematic form, which are more easily programmed for digital computers.

5.1.1 Mass matrix

All masses and mass moments of inertia entering the system of equations can be grouped in a single matrix [m] called the "mass matrix". For the coordinates chosen in section 3.2.1, the mass matrix results to be diagonal, reason for which the system is said to be "dynamically uncoupled". Coupling is not an inherent property of the structure but depends on the coordinates used to describe the motion.

Mass matrix (5.2) corresponds to the model shown in Figure 3.2. This matrix was assembled by lining up masses and mass moments of inertia for all masses in the system on the diagonal of an otherwise null matrix. The order to follow is given in Appendix C.

5.1.2 Global stiffness matrix

The assemblage of the stiffness matrix is not as straight forward as it was for the mass matrix. The stiffness matrix can be obtained from the system of equations resulting from application of Newton's 2nd. law, or Lagrange's equations, but these approaches lead to quite involved calculations.

A simpler and more systematic method exists to assemble the global stiffness matrix of the structure when it can be done in a digital computer. This is conveniently accomplished

programmed for digital computers.

$$
\begin{bmatrix}
m_h & & & & & & & & & & & \\
& m_h & & & & & & & & & & \\
& & I_h & & & & & & & & & \\
& & & m_{t1} & & & & & & & & \\
& & & & m_{t1} & & & & & & & \\
& & & & & I_{t1} & & & & & & \\
& & & & & & \ddots & & & & & \\
& & & & & & & m_{15} & & & & \\
& & & & & & & & m_{15} & & & \\
& & & & & & & & & I_{15} & & \\
& & & & & & & & & & m_{sp} & \\
& & & & & & & & & & & m_{sp} \\
& & & & & & & & & & & & m_{ut} \\
& & & & & & & & & & & & & m_{ut}
\end{bmatrix}
\qquad (5.2)
$$

m_h : Lumped mass of head and neck

I_h : Mass moment of inertia of head-neck about its center of gravity

m_{ti}: Mass of ith thoracic vertebra

I_{ti}: Mass moment of inertia of ith thoracic vertebra about its center of gravity

m_{li}: Mass of ith lumbar vertebra

I_{li}: Mass moment of inertia of ith lumbar vertebra about its center of gravity

m_{sp}: Lumped mass of sacrum and pelvis

m_{ut}: Lumped mass of upper torso and upper limbs

by superimposing the stiffness matrices of the individual deformable structural elements, Martin (1966), which will be called "element stiffness matrices". There is a total of 28 element stiffness matrices in the structure corresponding to: neck, 17 intervertebral joints, and 10 costo-vertebral joints.

A generic (6x6) element stiffness matrix that applies to all intervertebral joints is shown in matrix (5.3), where the parameters K_a, K_s, and K_b stand for axial, shear, and bending stiffness of the intervertebral joint respectively.

The angle θ_i made by the longitudinal axis of a vertebra and the z-axis varies along the spine. The angle $\bar{\theta}_i$, the longitudinal axis of the disc makes with the z-axis, is taken as the average of the angles corresponding to the two vertebrae enclosing the disc. The angle $\bar{\theta}_i$ is shown in Figure 3.3 as the angle made by the disc middle plane a-a and the x-axis.

Appendix D shows the steps followed in deriving the intervertebral joint stiffness matrix from the equations of static equilibrium. A similar procedure was followed to calculate the element stiffness matrices corresponding to neck, and costo-vertebral joints.

Since matrix (5.3) was derived using a convenient system of coordinates u, w, δ, Figure 3.6, which is not the global system x, z, δ, adopted for the derivation of the equations of motion (5.1), the intervertebral joint stiffness matrix $[k_1]$ must be subjected to a coordinate transformation, a

$$
\left[k_1\right] = \begin{bmatrix}
K_s & 0 & K_s Z_i \cos\theta_{12} & -K_s & 0 & -K_s Z_s \cos\theta_{12} \\
 & K_a & -K_a Z_i \sin\theta_{12} & 0 & -K_a & -K_a Z_s \sin\theta_{12} \\
 & & K_b + Z_i^2 \left[K_s \cos^2\theta_{12} + K_a \sin^2\theta_{12}\right] & -Z_i K_s \cos\theta_{12} & Z_i K_a \sin\theta_{12} & -K_b + Z_i Z_s \left[K_a \sin^2\theta_{12} - K_s \cos^2\theta_{12}\right] \\
 & & & K_s & 0 & K_s Z_s \cos\theta_{12} \\
 & & & & K_a & K_a Z_s \sin\theta_{12} \\
 & & \text{SYMMETRIC} & & & K_b + Z_s^2 \left[K_s \cos^2\theta_{12} + K_a \sin^2\theta_{12}\right]
\end{bmatrix} \qquad (5.3)
$$

rotation, that makes it suitable for assemblage into the global stiffness matrix $[k]$. The transformed matrix $[k_e]$ is obtained from equation (5.4) which involves the rotation matrix $[R]$ and its transpose $[R_t]$, Gere and Weaver (1965).

$$[k_e] = [R_t]^T [k_1] [R_t] \tag{5.4}$$

$$[R_t] = \begin{bmatrix} [R] & 0 \\ 0 & [R] \end{bmatrix} \tag{5.5}$$

$$[R] = \begin{bmatrix} \cos\bar{\theta} & -\sin\bar{\theta} & 0 \\ \sin\bar{\theta} & \cos\bar{\theta} & 0 \\ 0 & 0 & 1 \end{bmatrix} \tag{5.6}$$

5.1.3 Damping matrix

The same formulation developed for evaluation of the global stiffness matrix holds for the global damping matrix. The only difference being that stiffness coefficients must be replaced by corresponding damping coefficients.

5.2 Solution of the System of Governing Equations

One way to solve the system of equations (5.1) would be by finding a linear transformation of coordinates able to uncouple the system of equations. Every equation of the uncoupled system can be solved individually as normally done for a single degree of freedom system.

A relatively simple method was presented by Foss (1958)

to find a matrix of orthogonal eigenvectors able to uncouple the system of equations in an auxiliar system of coordinates. Integration of individual equations is then done for the forcing function of interest, and the auxiliary coordinates transformed back to the original system of generalized coordinates that have the physical meaning of interest.

The procedure just briefly introduced has the potential to provide the response of the system to different inputs. After the mass, stiffness and damping matrices are obtained, a dynamical matrix is assembled. The complex eigenvalues and eigenvectors of the dynamical matrix fully characterize the dynamic behavior of the system, so that its response can be calculated for a given excitation using the eigenvalues and eigenvectors as input data together with a short computation for integration of the uncoupled differential equations.

This approach was tried in the present work, but some inconsistencies were found in the results. The reason for such behavior probably being the existance of some errors in the eigenvectors as a result of the large number of degrees of freedom of the system with some eigenvalues not very distinct from each other.

The main objectives of this project are equally fulfilled by using a less general solution of the system of second order differential equations. The complementary solution of equations (5.1) is not of major interest in the present work.

If the vibrational input includes only sinusoidal oscillations, a particular solution as given by equation (5.7), Thomson (1972), Reismann and Pawlik (1975), will provide most of the answers sought. The particular solution consists of a set of functions $q_j(t)$ describing the steady state harmonic oscillation of the same frequency ω as that of the excitation. Each mass in the structure will oscillate about its equilibrium position with an amplitude $|A_j|$ and lagging the vertical motion of the base by an angle ψ_j which is related to the amount of damping existing between the excitation point and the point where the oscillation is being studied.

$$q_j\ (t) = |A_j|\ e^{i\,(\omega t + \psi_j)} \tag{5.7}$$

The response equations (5.7) and their derivatives can be written in a more suitable form for implementation of the solution of equation (5.1) in a digital computer. The phase angle is removed from the exponential factor and incorporated as a complex amplitude, A_j, equations (5.8) to (5.11).

$$q_j\ (t) = A_j\ e^{i\omega t} \tag{5.8}$$

$$A_j = A_j^r + i\ A_j^i \tag{5.9}$$

$$\dot{q}_j\ (t) = i\omega A_j\ e^{i\omega t} \tag{5.10}$$

$$\ddot{q}_j\ (t) = -\ \omega^2\ A_j\ e^{i\omega t} \qquad (5.11)$$

The base excitation $z_b(t)$, equation (5.12), applied in vertical direction (±z) to the pelvis of a seated operator is a displacement type excitation, so the forcing function f(t) entering equation (5.1) needs to be written in a different form to be able to characterize the excitation by a displacement amplitude and a frequency instead of a force amplitude and a frequency.

$$z_b\ (t) = A_b\ e^{i\omega t} \qquad (5.12)$$

A_b : Real amplitude of base harmonic motion

The forcing function f(t) is calculated from the equation of dynamic equilibrium (5.13) of forces acting on the operator seat in z-direction. The forces applied to the seat are: the action of the body f(t), plus those generated at the seat suspension as a result of its stiffness K_c, damping C_c, and the relative motion seat-base BS, Figure 5.1.

$$M_c\ \ddot{q}_s(t) = K_c\ BS + C_c\ \dot{BS} - f(t) \qquad (5.13)$$

The displacement of the seat is assumed to be that of the sacrum-pelvis mass $q_s(t)$, equation (5.14). This assumption

is valid for an operator seated on a bare seat where the stiffness of the tissues located between the pelvis and the seat is sufficiently high; about 1000 Kg/cm proved to give satisfactory results for the present model. No experimental data are available.

$$q_s(t) = A_s e^{i\omega t} \tag{5.14}$$

A_s : Complex amplitude of pelvis-sacrum oscillation

$$BS = z_b(t) - q_s(t) \tag{5.15}$$

From equations (5.12), (5.14), and (5.15) BS can be written:

$$BS = (A_b - A_s)\, e^{i\omega t} \tag{5.16}$$

Introducing equations (5.14) and (5.16) into (5.13) the forcing function can be written:

$$f(t) = \left[M_c \omega^2 A_s + K_c (A_b - A_s) + iC_c (A_b - A_s) \right] e^{i\omega t} \tag{5.17}$$

Separating the real part, F_s^r, and the imaginary part, F_s^i, of f(t),

$$f(t) = (F_s^r + iF_s^i)\, e^{i\omega t} = F_s e^{i\omega t} \tag{5.18}$$

$$F_s^r = K_c A_b + (\omega^2 M_c - K_c) A_s^r + \omega C_c A_s^i \tag{5.19}$$

$$F_s^i = (\omega^2 M_c - K_c) A_s^i - \omega C_c A_s^r + \omega C_c A_b \tag{5.20}$$

Substituting equations (5.8), (5.10) (5.11) and (5.18) in (5.1), after cancelling exponential factors the system of differential equations is turned into a system of algebraic equations:

$$-\omega^2[m]\{A\} + i\omega[c]\{A\} + [k]\{A\} = \{F\} \tag{5.21}$$

$\{A\} = \{A^r\} + i\{A^i\}$: Vector including complex amplitudes of oscillation for all degrees of freedon in the system.

$\{F\} = \{F^r\} + i\{F^i\}$: Vector including complex amplitudes of all external forces acting on the system.

Writing all amplitudes in complex form, equation (5.21) turns into (5.22).

$$-\omega^2[\ ]\{A^r\} - i\omega^2[m]\{A^i\} + i\omega[c]\{A^r\} - \omega[c]\{A^i\} + [k]\{A^r\} + i[k]\{A^i\} = \{F^r\} + i\{F^i\} \tag{5.22}$$

By equating real and imaginary parts of equation (5.22) the system of N equations with complex unknowns is turned into a system with 2N equations in all real numbers.

$$\begin{bmatrix} [k] - \omega^2[m] \end{bmatrix} \{A^r\} - \omega[c]\{A^i\} = \{F^r\} \tag{5.23}$$

$$\omega\,[c]\,\{A^r\} + \left[[k] - \omega^2[m]\right]\{A^i\} = \{F^i\} \qquad (5.24)$$

The dimension of vectors F^r and F^i is 58, but only one component is different from zero. It corresponds to the vertical motion of the sacrum, and is obtained from equations (5.19) and (5.20).

$$\begin{bmatrix} [k]-\omega^2[m] & \vdots & -\omega[c] \\ \cdots\cdots & \vdots & \cdots\cdots \\ \omega[c] & \vdots & [k]-\omega^2[m] \end{bmatrix} \begin{Bmatrix} A^r \\ A^i \end{Bmatrix} = \begin{Bmatrix} 0 \\ 0 \\ \vdots \\ 0 \\ F^r_s \\ 0 \\ 0 \end{Bmatrix} = \begin{Bmatrix} 0 \\ 0 \\ \vdots \\ 0 \\ F^i_s \\ 0 \\ 0 \end{Bmatrix}$$

$$= \begin{matrix} K_c \begin{Bmatrix} 0 \\ 0 \\ \vdots \\ 0 \\ A_b \\ 0 \\ 0 \end{Bmatrix} + (\omega^2 M_c - K_c)[I] \begin{Bmatrix} 0 \\ 0 \\ \vdots \\ 0 \\ A^r_s \\ 0 \\ 0 \end{Bmatrix} + \omega C_c [I] \begin{Bmatrix} 0 \\ 0 \\ \vdots \\ 0 \\ A^i_s \\ 0 \\ 0 \end{Bmatrix} \\ \omega C_c \begin{Bmatrix} 0 \\ 0 \\ \vdots \\ 0 \\ A_b \\ 0 \\ 0 \end{Bmatrix} + (\omega^2 M_c - K_c)[I] \begin{Bmatrix} 0 \\ 0 \\ \vdots \\ 0 \\ A^i_s \\ 0 \\ 0 \end{Bmatrix} - \omega C_c [I] \begin{Bmatrix} 0 \\ 0 \\ \vdots \\ 0 \\ A^r_s \\ 0 \\ 0 \end{Bmatrix} \end{matrix} \qquad (5.25)$$

There are two unknowns on the right side of equation (5.25) that must be moved to the left side of the equation to make the system suitable for computer solution. Equation (5.26) was used to program the assemblage and solution of the system of equations into subroutine "AMPLTD" of program "COLSOL".

$$\begin{bmatrix} [km] & -[\omega c] \\ [\omega c] & [km] \end{bmatrix} \begin{Bmatrix} A^r \\ A^i \end{Bmatrix} = A_b \begin{Bmatrix} 0 \\ \vdots \\ K_c \\ 0 \\ 0 \\ \vdots \\ \omega C_c \\ 0 \end{Bmatrix} \tag{5.26}$$

$$[km] = \left[[k] - \omega^2 [m]\right] + (K_c - \omega^2 M_c) \begin{bmatrix} 0 & & & & \\ & 0 & & & \\ & & 0 & & \\ & & & \ddots & \\ & & & & 1 \\ & & & & & 0 \\ & & & & & & 0 \end{bmatrix} \tag{5.27}$$

$$[\omega c] = \omega [c] - \omega C_c \begin{bmatrix} 0 & & & & \\ & 0 & & & \\ & & 0 & & \\ & & & \ddots & \\ & & & & 1 \\ & & & & & 0 \\ & & & & & & 0 \end{bmatrix} \tag{5.28}$$

5.3 Driving Point Impedance of the Model

The driving point impedance of the seated subject was used for validation of the model. Since no provisions were made to represent the rheological properties of the deformable elements existing between the sacrum and the seat, the seat suspension spring (K_c) and damper (C_c) were used to model the behavior of these elements in the validation process. If the mass of the seat, Figure 5.1, is assumed to be null and the base is thought as the seat surface, the seat suspension left in between them would simulate the behavior of the deformable elements separating the seat from the sacrum.

Under these assumptions the driving point impedance can be calculated from the velocity of the base, equation (5.29), and the force transmitted through the suspension, equation (5.17), which can be calculated after solving the system of equations (5.26).

$$V(t) = i\omega A_b e^{i\omega t} \tag{5.29}$$

The driving point impedance then results:

$$Z = (1 - A_s/A_b) \left[C_c - iK_c/\omega \right] \tag{5.30}$$

5.4 Shear and Axial Deformations of Intervertebral Joints

A general expression describing the motion of every mass in the structure is given by equations (5.8), which are

renamed according to the direction of motion as shown by equations (5.31) to (5.33) for horizontal, vertical, and rotational motion respectively.

$$x_j(t) = \bar{X}_j e^{i\omega t} \tag{5.31}$$

$$z_j(t) = \bar{Z}_j e^{i\omega t} \tag{5.32}$$

$$\delta_j(t) = \Delta_j e^{i\omega t} \tag{5.33}$$

$\bar{X}_j$, $\bar{Z}_j$, and Δ_j are complex amplitudes equivalent to A_j

The shear deformation, S, of an intervertebral joint is approximated by projecting all displacements of two adjacent vertebrae on the disc middle plane a-a, Figure 5.2. The axial deformation, N, is calculated by projecting all displacements in direction perpendicular to a-a.

$$S = \left[x_1(t) - x_2(t)\right] \cos\bar{\theta} - \left[z_1(t) - z_2(t)\right] \sin\bar{\theta} + \\ + \left[\delta_1(t)\, Z2 - \delta_2\, Z1\right] \cos\theta_{12} \tag{5.34}$$

$$N = \left[x_1(t) - x_2(t)\right] \sin\bar{\theta} + \left[z_1(t) - z_2(t)\right] \cos\bar{\theta} - \\ - \left[\delta_1(t)\, Z2 - \delta_2\, Z1\right] \sin\theta_{12} \tag{5.35}$$

$$S = \left\{ \left[\bar{X}_1 - \bar{X}_2 \right] \cos \bar{\theta} - \left[Z_1 - Z_2 \right] \sin \bar{\theta} + \right.$$

$$\left. + \left[\Delta_1 \, Z2 - \Delta_2 \, Z1 \right] \cos \theta_{12} \right\} e^{i\omega t} \qquad (5.36)$$

$$N = \left\{ \left[\bar{X}_1 - \bar{X}_2 \right] \sin \bar{\theta} + \left[\bar{Z}_1 - \bar{Z}_2 \right] \cos \bar{\theta} - \right.$$

$$\left. - \left[\Delta_1 \, Z2 + \Delta_2 Z1 \right] \sin \theta_{12} \right\} e^{i\omega t} \qquad (5.37)$$

θ_{12} : Angle made by vertebra end plate and disc middle plane a-a

5.5 Seat to Head Transmissibility

The seat to head transmissibility is defined as the ratio between the acceleration of the head and the input acceleration through the pelvis. For harmonic motion the ratio of accelerations is equivalent to the ratio of displacements.

Considering the same assumptions made for evaluation of driving point impedance, that is, null seat mass and seat suspension representing the deformable elements located between sacrum and seat surface, the transmissibility Tr is as given by equation (5.38).

$$Tr = \frac{\bar{Z}_{head}}{A_b} \qquad (5.38)$$

$\bar{Z}_{head}$: Complex amplitude of head vertical motion

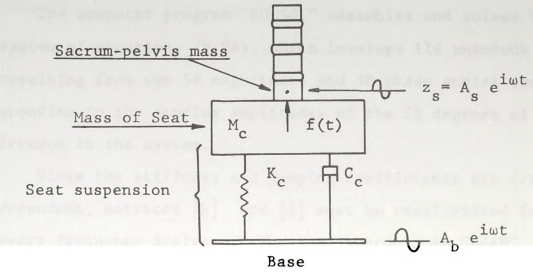

Figure 5.1. Operator seat under sinusoidal displacement excitation.

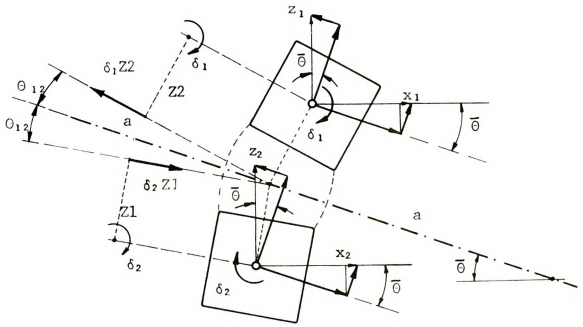

Figure 5.2. Displacements and rotations of two consecutive vertebrae determine the axial and shear deformations of the enclosed intervertebral joint.

5.6 Computer Program

The computer program "COLSOL" assembles and solves the system of equations (5.26), which involves 116 unknowns resulting from the 58 magnitudes and 58 phase angles corresponding to the complex amplitudes of the 58 degrees of freedom in the system.

Since the stiffness and damping coefficients are frequency dependent, matrices $[k]$ and $[c]$ must be recalculated for every frequency analyzed. The same subroutines "HEAD", "DISC" and "THORAX" are involved in the calculation of both matrices. Before the computation of $[k]$ all frequency dependent stiffness coefficients are calculated by calling subroutine "CALKDZ". Similarly, before the computation of $[c]$, subroutine "CALCDZ" is called to calculate all frequency dependent damping coefficients.

After all required matrices have been calculated, subroutine "AMPLTD" is called to assemble and solve the system of equations (5.26). With all amplitudes and phase angles already known, subroutine "OUTOUT" is called to calculate and print seat to head transmissibility, equation (5.38), and driving point impedance, equation (5.30), which are used for validation of the model. Subroutine "OUTPUT" will also calculate and print axial and shear intervertebral joint deformations, equations (5.36) and (5.37), which are the response parameters of interest after the model has been validated.

The flow chart shown in Figure 5.3 summarizes the steps described in the previous paragraphs.

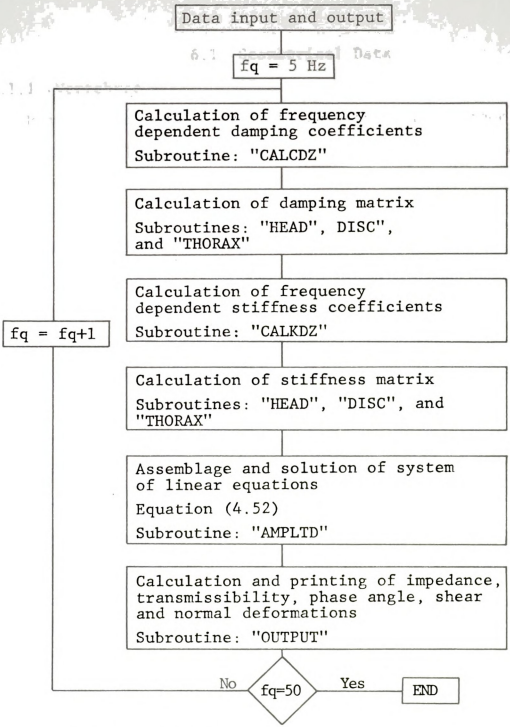

Figure 5.3. Flow chart for computer program "COLSOL".

VI. EXPERIMENTAL DATA

6.1 Geometrical Data

6.1.1 Vertebrae

Most of the geometrical data required for a lumped parameter model of the spine is available in the literature. The curvature of the spine in the sagittal plane, Table 6.1, was calculated from the coordinates (u_0, w_0) reported by Orne and King Liu (1971) for a seated position.

The existing data on dimensions of vertebrae, such as that given by Lanier (1939), does not include values of mass of individual vertebra or location of its center of gravity. Approximation of the geometry of a vertebra by superposition of bodies of known configuration, such as a truncated cone or an ellipsoid was considered, but it presents some difficulties. For instance there is enough variation of vertebra configuration through the thoracic spine to justify the use of more than one model. The cross section of the vertebral body at the first thoracic vertebra is approximately trapezoidal, toward the fifth vertebra the body cross section becomes approximately parabolic. The geometry of vertebrae significantly changes when passing from the thoracic to the lumbar spine so at least three different models would be required to be able to calculate the properties such as center of gravity and moment of inertia for the thoracic spine.

Table 6.1. Curvature of the thoracolumbar spine in the sagittal plane.

$$\theta_i = \arctan\left(\frac{u_{(i+1)} - u_{(i)}}{w_{(i+1)} - w_{(i)}}\right)$$

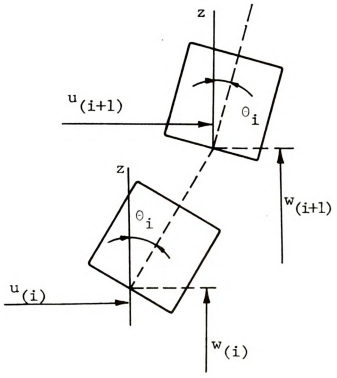

Vertebral Level	θ Deg.
Th1	5.0(1)
Th2	9.8
Th3	17.4
Th4	14.9
Th5	12.5
Th6	0.0
Th7	-4.6
Th8	-8.3
Th9	-15.1
Th10	-15.2
Th11	-14.0
Th12	-18.7
L1	-16.8
L2	-10.6
L3	-2.2
L4	4.7
L5	14.2
Sacrum	45.0(2)

(1) Arbitrary

(2) Kazarian (1972): 45.0 deg.; Schultz et al. (1973): 32.5 deg.

Even if the geometry of a vertebra coul be reasonably approximated, there still remains the problem of estimating the density distribution over the volume of the vertebra. The end plates have different density from the nucleus of the spongy vertebral body or the transverse processes.

Due to the problems previously stated, the geometrical properties of the thoracic and lumbar vertebrae were determined experimentally. A spine (C2 to L5) was removed from an embalmed cadaver provided by the Anatomy Laboratory of Michigan State University. The spine was considered normal, with larger dimensions than the average reported by Lanier (1939).

The moisture content was maintained by wrapping the spine in a moist cloth and sealing it in a polyethylene bag to avoid any drying that could change the mass or density distribution within each vertebra; such changes would affect the values of mass moment of inertia to be measured. The dimensions measured on each vertebra are listed in Table 6.2. The coordinates of the costo-vertebral joints are given in the table, but were not used for the final version of the model.

The location of the center of gravity in the mid-sagittal plane was determined experimentally using the pendulum built to measure mass moment of inertia, Figure 6.1. The vertebra was hung from the pendulum frame by means of a thin spring wire, .5 mm in diameter. The wire was soldered to a tiny

Table 6.2. Geometrical data for thoracic and lumbar vertebrae.

Vertebra	Z1	Z2	Xi	Zi	Xs	Zs	Xt	Zt
	cm							
T1	1.2	-1.2	1.0	1.4	-1.2	-0.9	-1.1	0.8
T2	1.2	-1.3	0.9	1.3	-1.0	-0.9	-1.8	0.8
T3	1.5	-1.3	0.7	1.1	-0.7	-0.7	-1.7	0.8
T4	1.5	-1.3	0.5	0.9	-0.3	-1.3	-2.3	0.8
T5	1.5	-1.3	0.5	0.9	-0.1	-1.0	-2.3	0.8
T6	1.5	-1.3	0.2	1.2	-0.1	-0.9	-2.4	1.0
T7	1.7	-1.3	0.1	1.3	0.0	-1.0	-2.5	1.1
T8	2.0	-1.0	-0.2	1.5	-0.1	-0.9	-2.5	0.9
T9	2.0	-1.3	0.0	1.6	0.0	-1.0	-2.4	0.5
T10	1.8	-1.6	-0.3	1.0	-0.1	-1.4	-2.5	0.3
T11	1.9	-1.7	-0.6	0.3	-0.4	-1.3	-2.3	0.0
T12	2.0	-1.7	-	-	-	-	-	-0.5
L1	2.1	-1.6	-	-	-	-	-	-
L2	2.1	-1.7	-	-	-	-	-	-
L3	2.2	-1.7	-	-	-	-	-	-
L4	2.2	-1.8	-	-	-	-	-	-

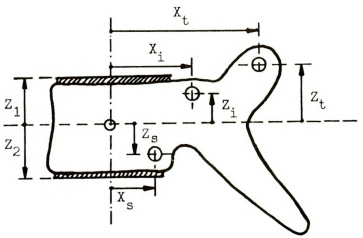

wood screw (5 mm long) at one end, and to a piece of razor blade in the opposite end. The total weight of the support wire is .42 gm.

Every vertebra was hung from two different points in the mid-sagittal plane, and a vertical line passing through the pivot point was drawn for each hanging position. The point of intersection of these lines corresponds to the location of the center of gravity. The distance "r" from the pendulum pivot to the center of gravity as well as the location of the costo-vertebral points of interaction were then measured, see Table 6.3.

6.1.2 Head and neck

In the absence of experimental data, the location of the lower end plate of the seventh cervical vertebra is assumed to be 17 cm below and 3.8 cm behind the center of gravity of the head-neck system, see Figure 6.3. Orne and King Liu (1971) reported satisfactory dynamic model results using a head neck eccentricity of 3.8 cm.

6.1.3. Pelvis

The sacrum-pelvis mass is included in the model with only two degrees of freedom according to the assumptions made in section 3.2. Therefore no geometrical data is required other than the angle the axis of the sacrum makes with the z-axis, which is given in Table 6.1.

6.2 Mass Moment of Inertia of a Vertebra

Rotation in the sagittal plane is one of the degrees of

freedom considered in the model. The mass moment of inertia of each vertebra with respect to its center of gravity in the sagittal plane is required to write the equation corresponding to the rotational mode of oscillation.

The moments of inertia of the thoracic and lumbar vertebrae were calculated from the period of oscillation of the vertebra in pendular motion in the mid-sagittal plane. The pendulum, Figure 6.1, was constructed and then tested for bodies of regular geometry (cylinder, ring) in order to verify the concepts described in the next paragraphs, particularly those relating to the accuracy required to measure the time period and the distance from the pivot point of the pendulum to the c.g. of the oscillating body.

The moment of inertia, I_g, can be calculated from the natural frequency of oscillation of the pendulum, Martin (1969). The natural frequency, equation (6.1), is obtained from the solution of the pendulum differential equation of motion.

$$Ig = W\, r \left[\left(\frac{T}{2\P} \right)^2 - \frac{r}{g} \right] \qquad (6.1)$$

T: Period of oscillation of the pendulum

r: Distance from pivot point to center of gravity of oscillating vertebra.

The coefficients of sensitivity of the moment of inertia with respect to the period "T" and the radius "r" can be

written:

$$S_t = \frac{100}{I_g} \frac{\partial I_g}{\partial T} = 100 \left[\frac{2\, g\, T}{g\, T^2 - 4\, r \pi^2} \right] \qquad (6.2)$$

$$S_r = \frac{100}{I_g} \frac{\partial I_g}{\partial r} = 100 \left[\frac{1}{r} + \frac{4\, \pi^2}{4\, r\, \pi^2 - g\, T^2} \right] \qquad (6.3)$$

A .01 sec. error in measuring T, could give an error as high as 120% for I_g. A 1.0 mm error in measuring r could give an error as high as 34% for I_g. These figures are calculated from equations (6.2) and (6.3) together with data from Table 6.3. The period of oscillation must be measured to within .001 sec to keep the error of I_g below 12%.

The pendulum was first run at atmospheric pressure in an environment with apparently no air circulation. The variability among readings of T (over 2%) was considered too high. By enclosing the pendulum in a glass chamber under 500 mm of vacuum, Figure 6.2, the variability of T was reduced to 0.1%. Even though it can lead to errors as high as 12% for I_g, the final results can still be within what could be expected for a biological material.

It was found that in order to take the variability of T to within 0.1% the time period should be averaged over at least 500 oscillations. An electric counter activated by a photo-relay was used to keep track of the number of oscillation. The time elapsed was measured with a stop watch.

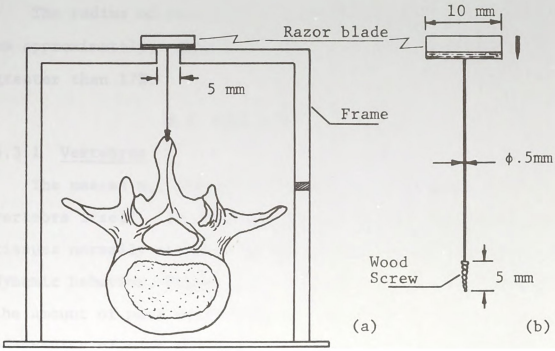

Figure 6.1. a) Pendulum to measure mass moment of inertia
b) Support of vertebra

Figure 6.2. Pendulum installed in vacuum chamber to minimize error due to air friction.

The radius of oscillation, r, was measured to within 0.5 mm approximately. This resulted in an error for I_g no greater than 17%.

6.3 Masses in the System

6.3.1 Vertebrae

The masses m_j, listed in Table 6.3, correspond to the vertebra itself. It does not include any of the peripheral tissues normally attached to the spine that contribute to its dynamic behavior, Figure 6.4. In order to be more realistic the amount of mass to be ideally concentrated at the center of gravity of each vertebra must be increased so that the material most closely attached to the vertebrae and that actually follows its motion is taken into account.

A total mass of 7712 gm, Muksian and Nash (1974) was adopted for the spine and most closely attached ligaments and muscle tissues. The distribution of the back mass on the centers of gravity of the thoracic and lumbar vertebrae was assumed to be proportional to the mass of each vertebra as given by equation (6.4).

$$m'_j = 7712 \times \frac{m_j}{\Sigma m_j} \qquad (6.4)$$

The numerical values are shown in Table 6.3. The mass distribution just described is satisfactory for the lumbar spine where the mass enclosed in the abdomen can be considered to be resting directly on the bony basin presented by the

Table 6.3. Mass and mass moment of inertia respect to the center of gravity of thoracic and lumbar vertebrae.

Age = 51 Sex = Male Cause of death = cardiac arrest

Body weight: 85 Kg(1) Body height: 1.82 m(1)

Vertebral level	m_j	m'_j	r	T	$Ig_{(y)}$	
	grams		cm	sec	gm.cm²	
T1	48.5	272.3	12.66	.722	175.61	
T2	45.4	254.9	12.44	.724	326.34	
T3	42.1	236.4	12.59	.727	284.06	
T4	46.4	260.5	12.69	.730	320.60	
T5	47.0	263.9	12.94	.732	223.26	
T6	51.8	290.8	12.94	.734	294.87	
T7	55.0	308.8	11.79	.710	472.88	
T8	62.5	350.9	11.84	.720	765.44	
T9	66.6	373.9	11.84	.717	731.23	
T10	74.3	417.2	11.44	.704	738.25	
T11	81.0	454.8	11.39	.703	815.20	
T12	93.0	522.2	11.34	.702	947.79	
L1	106.5	598.0	11.66	.711	1110.82	
L2	125.3	703.5	12.36	.726	1130.32	
L3	140.2	787.2	12.49	.731	1367.2	
L4	147.7	829.3	12.59	.733	1401.14	
L5	140.2	787.2	-	-	1367.2	(2)

m_j: mass of vertebra
m'_j: mass of vertebra plus more closely attached tissues
r : radius of oscillation (pendulum)
T : period of oscillation
I_g: mass moment of inertia

(1): Estimate ; (2) : Arbitrary value.

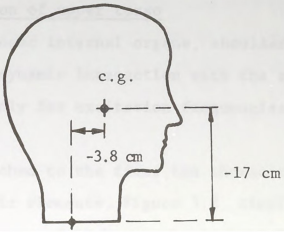

Figure 6.3. Location of the point of interaction of the head-neck lumped mass with the upper end of the spine.

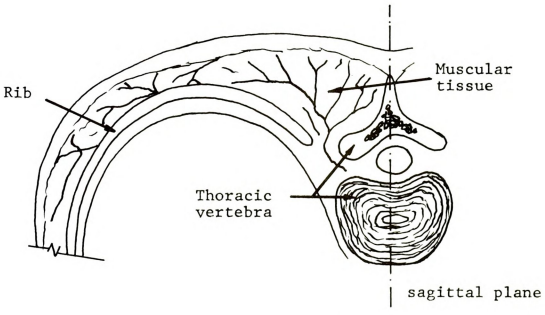

Figure 6.4. A fraction of the back muscles and other tissues are closely attached to the spine.

pelvis without any significant dynamic interaction with the spine. The thoracic mass requires special consideration.

6.3.2 Suspended portion of upper torso

The rib cage, enclosed internal organs, shoulders and arms have significant dynamic interaction with the spine of a seated operator, mainly for excitation frequencies below 15 Hz.

A single mass attached to the first ten thoracic vertebrae by means of viscoelastic elements, Figure 3.2, simulates the action of the upper torso and limbs on the spine well enough to give plots of seat to head transmissibility as well as driving point impedance close to experimental measurements.

The suspended mass of the thorax can be estimated from the weight distribution for head and upper torso shown in Table 6.4.

Both arms and shoulders	9981.0 gm
Thoracic organs, blood and diaphragm	4354.0 gm
Ribcage and muscles	16838.0 gm
Suspended thoracic mass	31173.0 gm

This mass should be reduced as a result of the arms not being supported by the spine alone, and a fraction of the mass of thoracic organs, blood, muscles, and diaphragm being directly attached to the spine.

Part of the weight of the arms rests on the legs according to the posture assumed by the subject in the transmissibility

and impedance tests reported by Pradko et al. (1967), which are used for validation of the model. It is also the situation of a machine operator with the arms resting on the steering wheel. From these consideration it was decided to reduce the suspended thoracic mass from 31,173 gm to 20,000 gm.

6.3.3 Head and neck

Head and neck are included in the model as a compounded mass of 6078.0 gm, Table 6.4. The mass moment of inertia about the center of gravity was adopted from Liu et al. (1971).

(Mass moment of inertia of head + C1-T1)$_{c.g.}$ = 20.56×10^5 gm cm^2.

Similar results were reported by Vulcan and King (1971); the data obtained from 3 cadavers are: 21.1×10^5; 22.76×10^5 and 39.02×10^5 gm cm^2.

6.3.4 Sacrum-Pelvis

The magnitude of the mass attached to the lower end of the spine will affect the values of driving point impedance of the model, which are compared with experimental values for validation of the model dynamic behavior.

Assuming the total weight of the abdomen plus 45% of the pelvis-legs weight as being directly interacting with the operator seat, the sacrum-pelvis mass can be calculated from Table 6.4.

Mass of sacrum-pelvis = 6623.0 + .45 × 30394.0 = 20300.0 gm

Table 6.4. Body weight distribution used for the model.

Element	Weight		Mass[5]
	lb.	Dyn ($\times 10^5$)	gm ($\times 10^2$)
Head and neck[2]	13.40	59.60	60.78
Both arms and shoulders[3]	22.00	97.86	99.81
Back[1]	17.00	75.62	77.12
Thoracic organs blood and diaphragm[2]	9.60	42.70	43.54
Ribcage and muscles in thorax[4]	37.12	165.12	168.38
Abdomen[1]	14.60	64.94	66.23
Pelvis and legs[1]	67.0	298.04	303.94
Total	180.72	804.0	820.00

(1) Muksian and Nash (1974).

(2) Payne (1970).

(3) Modified from Payne (1970) to include weight of shoulders.

(4) Modified from Payne (1970).

(5) All values taken from literature were multiplied by a factor:

Factor = (82000/reported body weight in grams).

	Weight	Mass (2)

6.4 Rheological Behavior of Deformable Elements

6.4.1 Intervertebral joints. Axial.

Three stiffness and damping coefficients are needed to characterize the rheology of the three modes of motion of each intervertebral joint. The coefficients entering the Kelvin elements that model the axial behavior of the disc are calculated from equations (4.20) and (4.21) together with the parameters shown in Table 6.5. These coefficients have been calculated from the impedance data collected by Kazarian (1972) using the loading frame shown in Figure 6.5.

The vertebral unit to be tested is placed between the superior and inferior loading heads. The upper head was designed in a manner so that a pure compression load could be applied. The compression bias was adjusted by slowly rotating the loading screw until the designated preload value was registered on the strip chart recorder.

The impedance and phase angle data reported were calculated from force and velocity recordings taken from the load and velocity transducer located underneath the lower loading head. The data obtained with the experimental set up just described corresponds to the axial mode of oscillation.

The exponential functions used to model stiffness and damping frequency dependent coefficients present short intervals within the range 5-50 Hz where the experimental points separate from the curve. For most frequencies the curves fit very well the experimental data as indicated by

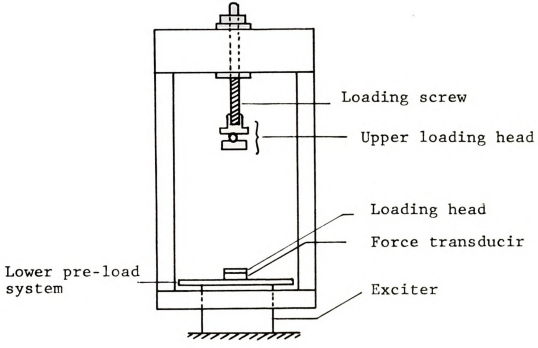

Figure 6.5. Loading frame for impedance testing, Kazarian (1972).

the coefficients of correlation and standard error of estimate given in Table 6.5.

The lumbar spinal units, which are shorter, only three vertebrae, present the largest deviations from the prediction curve. The reason for this behavior most likely being the existence of errors in the data, mainly phase angle, which is difficult to measure at resonant points where large changes of angle take place for small changes in frequency.

6.4.2 Intervertebral joints. Bending

There are no data available to model the bending and shear stiffness coefficients as functions of frequency as it was the case for the axial mode of deformation. It is reasonable to expect that similar frequency dependent parameters would be required for the shear and bending modes of deformation when modeled by Kelvin viscoelastic elements.

The bending stiffness coefficients were adopted from Markolf and Steidel (1970) for the thoraco-lumbar spine, T7 - L4:

Bending stiffness = $(3884.11 - 23304.68) \times 10^5$ dyn.cm/rad

These values do not show any significant variation with disc level. One might expect lumbar intervertebral joints to be stiffer due to the larger cross-sectional area, but the increased lumbar disc height compensates that factor making the bending stiffness approximately constant.

These data were obtained using free vibration tests carried on a single intervertebral joint. A resonant mass

Table 6.5. Parameters for estimation of frequency dependent stiffness and damping coefficients. Experimental data from Kazarian (1972). Axial mode of oscillation.

Vertebral level	Age group	k_1 ($\times 10^5$)	k_2 ($\times 10^{-2}$)	r	SE	c_1 ($\times 10^5$)	c_2	r	SE
T1-T6	G_1	20874.1	2.14	.96	8.93	265.78	-.590	.99	4.42
	G_2	30847.46	3.10	.94	12.67	320.56	-.466	.99	5.30
	G_3	25317.22	3.88	.95	20.78	155.83	-.193	.92	6.48
T7-T12	G_1	-	-	-	-	-	-	-	-
	G_2	22474.09	2.57	.99	3.06	352.48	-.623	.96	12.61
	G_3	33112.11	2.43	.95	11.36	322.04	-.524	.96	11.50
L1-L3	G_1	8348.3	1.24	.98	5.15	117.65	-.718	.99	6.41
	G_2	11335.2	1.89	.95	9.71	137.38	-.635	.99	5.96
	G_3	13577.17	2.05	.96	8.32	163.68	-.615	.99	3.72
L4-S	G_1	4285.51	1.77	.95	8.23	55.99	-.692	.94	18.90
	G_2	9532.52	1.35	.95	6.71	136.84	-.739	.99	6.86
	G_3	6731.45	1.40	.99	2.22	82.83	-.685	.97	11.81

$k = k_1 e^{k_2 fq}$; r : Coefficient of correlation

$c = c_1 (fq)^{c_2}$; SE: Standard error of estimate

was attached to the upper vertebra whose oscillations were recorded. The stiffness was calculated from the measured natural frequency of oscillation, while the damping factor was estimated from the rate of decay of the vibration trace.

The frequency of free oscillation corresponding to the single specimen in bending was 36.7 Hz, so it can be expected that bending stiffness will be lower for lower frequencies and higher for higher frequencies. No compression bias was used for the tests carried out by Markolf and Steidel (1970), so that an intervertebral joint under real loading conditions would have higher stiffness than those that resulted from the tests.

Assuming that the stiffness of the intervertebral joint under normal loading conditions is equal to the top value in the interval, (23304.68×10^5 dyn.cm/rad), and adopting the exponent factors k_2 corresponding to axial stiffness from Table 6.5, the coefficients k_1 for all units of the spine can be calculated, Table 6.6. The coefficients corresponding to the thoracic spine were increased by 150% to take into account the higher stiffness the ribcage gives to this portion of the spine, Prasad and King (1974). Only coefficient k_1, of formula (4.20) was modified ($9074.4 \times 2.5 = 22686.0$), and the same value was used for both halves of the thoracic spine.

In all cases the frequency used for the calculations is 36.7 Hz because it is the frequency at which the reported stiffness were measured.

Very little data are available in the literature on

damping coefficients of intervertebral joints for bending mode of oscillation. Prasad and King (1974) reported the following bending damping coefficients:

$$(\text{Bending damping})_{T1 - T10} = 226.0 \times 10^5 \text{ dyn.cm.sec/rad}$$

$$(\text{Bending damping})_{T11 - S} = 113.0 \times 10^5 \text{ dyn.cm.sec/rad}$$

These coefficients are not experimental; they were approximated in the process of optimizing the response of a lumped parameter model to transient vertical accelerations. The larger damping coefficients corresponding to the thoracic spine are in agreement with the results obtained for axial mode of oscillation from impedance data.

The frequency dependent damping coefficients for bending are calculated from equation (4.20). The coefficients previously introduced from Prasad and King are assigned to an intermediate frequency, 25 Hz. The parameters c_1 are then calculated for each one of the four thoraco-lumbar units using the exponents c_2 obtained from the impedance data for axial mode of oscillation, Table 6.5. The results are shown in Table 6.6.

6.4.3 Intervertebral joint. Shear

No direct measurements of shear stiffness are reported in the literature. Some insight into the shear behavior of the intervertebral joints can be obtained from Orne and King Liu (1971) through their analysis of the data reported by Evans and Lissner (1959). The basic data consist of load deflection

Table 6.6. Parameters for estimation of frequency dependent stiffness coefficient k, and damping coefficient c. Bending mode of oscillation.

Vertebral level	Age group	k_1 ($\times 10^5$)	k_2 ($\times 10^{-2}$)	c_1 ($\times 10^5$)	c_2
T1-T6	G_1	10865.7	2.14	584.1	-0.590
	G_2	7470.0	3.10	478.4	-0.466
	G_3	5610.8	3.88	308.3	-0.193
T7-T12	G_1	-	-	-	-
	G_2	9074.4	2.57	616.0	-0.623
	G_3	9552.9	2.43	525.2	-0.524
L1-L3	G_1	14784.4	1.24	717.7	-0.718
	G_2	11646.7	1.89	628.0	-0.635
	G_3	10982.5	1.05	608.1	-0.615
L4-S	G_1	12171.1	1.77	688.3	-0.692
	G_2	14199.4	1.35	742.4	-0.739
	G_3	13941.3	1.40	680.6	-0.685

$k = k_1 e^{k_2 fq}$ dyn.cm/rad

$c = c_1 (fq)^{c_2}$ dyn.cm.sec/rad

curves for thoracic and lumbar spine under bending in the sagittal plane.

The effective area, A_e, and the effective area moment of inertia, I_e, are unknown, so the values associated with the cross-section of the vertebral body were used for the calculations. The shape factor for the disc, k_s, lies somewhere between that of a solid circular section ($k_s = 1.25$) and that of a thin-walled circular section ($k_s = 2.0$).

$$\text{Shear stiffness} = \frac{12\ E\ I_e}{l^3\ (4\zeta - 3)} \tag{6.5}$$

$$\zeta = 1 + \frac{3\ E\ I_e\ k_s}{G\ A_e\ l^2} \tag{6.6}$$

$G = 1516.85 \times 10^5$ dyn/cm^2; $E = 4550.78 \times 10^5$ dyn/cm^2; $k_s = 1.5$

The shear stiffness coefficients resulting from equation (6.5) are shown in Table (6.7).

The data reported by Schultz et al. (1973), Appendix C, show significantly lower values. Even though these data correspond to intervertebral discs alone, no posterior aspects, it still gives a word of warning for the data in Table (6.6), which will only be considered as an upper bound for shear stiffness.

A stiffness frequency dependence of the type given by equation (4.21) was adopted for the shear mode of oscillation.

The thoracic and lumbar spine were divided in four parts as follows: T1-T6; T7-T12; L1-L3 and L4-S. All the intervertebral joints in one unit were assigned the same stiffness coefficient, so the values in Table 6.7 are averaged for each vertebral unit. The resulting stiffness together with the exponents, k_2, corresponding to the axial mode, Table 6.5, were used to evaluate k_1 from equation (4.21).

Since the data in Table 6.6 is on the high side, it will be associated with the highest frequency, 50 Hz, in the interval under consideration. An example is given below for the evaluation of the parameter k_1 corresponding to the top half of the thoracic spine for age group G1. A similar procedure is applied to the remaining units of the spine, see Table 6.8.

$$\frac{(20426.91 + ... + 22672.91)}{5} \times 10^5 = 23324.5 \times 10^5 =$$

$$= k_1 \, e^{0.0214 \times 50}$$

It follows that,

$$k_1 = 8000.5 \times 10^5$$

No data are available on damping for shear mode of oscillation, so the coefficients calculated for axial mode are used for shear as well.

Table 6.7. Shear stiffness of intervertebral discs of thoracic and lumbar spine.

Disc level	A_e	l	I_e	Shear stiffness (1)
	cm^2	cm	cm^4	dyn/cm ($\times 10^{+5}$)
T1	5.68	0.20	1.00	20426
T2	6.06	0.30	1.18	22179
T3	6.58	0.30	1.37	24337
T4	7.22	0.30	1.58	26089
T5	7.74	0.30	1.91	24240
T6	8.39	0.35	2.5	22672
T7	8.52	0.38	2.7	23338
T8	8.77	0.38	3.33	25227
T9	9.48	0.38	4.03	23070
T10	9.81	0.43	4.24	27914
T11	11.87	0.43	4.78	18102
T12	12.71	0.71	4.95	13188
L1	12.52	0.96	5.62	14480
L2	14.32	1.00	7.03	15876
L3	15.74	1.00	11.73	15916
L4	17.16	1.22	9.15	14223
L5	17.55	0.91	12.73	19502

A_e : effective area

I_e : effective area moment of inertia

l : height of intervertebral disc

(1) Data approximated following Orne (1970)

Table 6.8. Parameters for estimation of frequency dependent stiffness coefficient k and damping coefficient c. Shear mode of oscillation.

Vertebral level	Age group	k_1 ($\times 10^5$)	k_2 ($\times 10^{-2}$)	c_1 ($\times 10^5$)	c_2
T1-T6	G_1	8000	2.14	265.78	-0.590
	G_2	4950	3.10	320.56	-0.465
	G_3	3351	3.88	155.83	-0.193
T7-T12	G_1	-	-	-	-
	G_2	6032	2.57	352.48	-0.622
	G_3	6470	2.43	322.04	-0.523
L1-L3	G_1	8297	1.24	117.65	-0.718
	G_2	5995	1.89	137.38	-0.634
	G_3	5534	2.05	163.68	-0.614
L4-S	G_1	6959	1.77	55.90	-0.692
	G_2	8585	1.35	136.84	-0.739
	G_3	8373	1.40	82.83	-0.685

$k = k_1 e^{k_2 fq}$ dyn/cm

$c = c_1 (fq)^{c_2}$ dyn.sec/cm

6.4.4 Costo-vertebral joints

Most of the dynamic interaction between the upper torso and the thoracic spine takes place at the costo-vertebral joints. Some data is available on the rheological behavior of the transverse, inferior and superior costo vertebral joints. Andriacchi et al. (1974) reported experimental values of axial, shear and bending stiffness. These data are more applicable to a static, large deformation type of analysis.

Since this work is mainly focused on the lower part of the spine, the interaction spine-thorax was modeled in a simpler way following the description in Chapter III.

Muksian and Nash (1974) developed a lumped parameter model to study the response of seated humans to sinusoidal displacements of the seat. The spine was modeled as a rigid body attached to the pelvis through a linear spring and a linear dashpot. The thoracic cage was modeled as a rigid mass attached to the thoracic spine through a non-linear spring and a non-linear dashpot. The non-linearity is given by a term proportional to a cubic power of the spring elongation or it first derivative (dashpot), which are negligible for small deformations.

$(\text{Stiffness thorax - spine})_z = 525{,}42 \times 10^5$ dyn/cm

$(\text{Damping thorax - spine})_z = 38 - 54 \times 10^5$ dyn.sec/cm

Since the thorax is going to interact mainly with the first ten thoracic vertebrae, the stiffness and damping coefficients representing the interaction at each costovertebral joint can be taken as 1/10 of the values adopted from Muksian and Nash.

$(\text{Stiffness costovertebral joint})_z = 52.54 \times 10^5$ dyn/cm

$(\text{Damping costovertebral joint})_z = 3.8 - 5.4 \times 10^5$ dyn.sec/cm

The critical damping corresponding to the oscillating system representing the thorax can be obtained from the formulation for single degree of freedom systems:

Critical damping: $2\sqrt{k\,m} = 2\sqrt{525.42 \times 31173.0} = 25.6 \times 10^5$ dyn.sec/cm.

So the damping range previously adopted corresponds to an overdamped system. The value giving the best model response was 5.0×10^5 dyn.sec/cm.

6.4.5 Head and neck

The cervical spine consists of seven vertebrae separated by intervertebral joints and surrounded by ligaments and muscles. The neck can be then considered as a viscoelastic element linking the head to the upper end of the thoracic spine.

Payne and Band (1969), reported an undamped natural frequency of the head and neck, $f_n = 192.3$ rad/sec (30 Hz), from which a stiffness coefficient for the neck was approximated.

$\text{Mass}_{(\text{head + neck})} = 6078.0$ gm

$\text{Stiffness}_{(\text{neck})} = \text{Mass} \times f_n^2 = 6078.0 \times (192.3)^2 =$

$= 2248.0 \times 10^5$ dyn/cm

$\text{Critical damping}_{(\text{head + neck})} = 2 \text{ Mass } f_n = 23.38 \times 10^5$ dyn.sec/cm

From the data on stiffness reported by Prasad and King (1974) for the cervical spine the following value of stiffness was calculated:

$\text{Stiffness}_{(\text{neck})} = 708.33 \times 10^5$ dyn/cm

The model presented by Muksian and Nash (1974) reached satisfactory results using the following parameters for the Kelvin model:

$\text{Stiffness}_{(\text{neck})} = 525.42 \times 10^5$ dyn/cm

$\text{Damping}_{(\text{neck})} = 35 - 54 \times 10^5$ dyn.sec/cm

From the previous data the following ranges of variation for damping and stiffness of the neck were adopted.

$\text{Stiffness}_{(\text{neck})} = 500 - 700 \times 10^5$ dyn/cm

$$\text{Damping}_{(\text{neck})} = 30 - 50 \times 10^5 \text{ dyn.sec/cm}$$

VII. RESULTS AND DISCUSSION

7.1 Validation of the Model

The main objective of the model proposed in Chapter III is prediction of intervertebral joint deformations. Direct laboratory measurements of such deformations would be the ideal way to validate the model. Since these measurements are possible but not feasible with the present state of transducer design, alternative indirect validation techniques were used. Mechanical driving point impedance and seat-to-head transmissibility are two techniques described by Hopkins (1970), that were adopted for validation of the model under investigation.

Mechanical impedance and transmissibility are two well known tools for studying the dynamic response of biological systems. A seated human subject can be considered a "black box" much as one would an unkown electrical circuit. The response of the system is described by the location of resonant points as well as the magnitude of the impedance or transmissibility vectors over the frequency range.

The mechanical impedance gives an indication of the model behavior at one end of the torso, the pelvis; the coefficient of transmissibility indicates the response at the opposite end, the head. If both ends of the model (head and pelvis) have a response close to the experimental values, it is

reasonable to expect that the assuptions made to model the structure located in between those two points must be close to the real situation.

Impedance-frequency curves can be obtained from transient loading conditions using Fourier analysis, Weis et al. (1966), Sandover (1970), or a more direct method, called steady determination, that includes measurements of force and velocity for discrete values of frequency over the range of interest, Coermann (1963), Pradko et al. (1967). The results of steady state and transient impedance determinations reported by Weis et al. (1966) show some unexplained discrepancies, so the data reported by Pradko et al. (1967), from steady state tests, will be used for validation of the model.

There are three reasons for choosing Pradko's data over other impedance curves existing in the literature:

a. The data cover the full frequency range of interest
b. The impedance curves are the mean of different acceleration levels
c. The measurements were made using sinusoidal excitation (steady state), which is the situation being studied with the model.

The driving point impedance curve of the model is shown in Figure 7.1 together with the experimental curve reported by Pradko et al. (1967). These data are in good agreement with measurements made by Suggs et al. (1969) on 11 subjects for frequencies under 10 Hz. The impedance data reported by Coermann (1963) show a much higher maximum between 4 and 5

Hz. However the general shape of the curve is the same.

Even though the exponential functions, (4.20) and (4.21), giving the stiffness and damping coefficients are based on data in the range 5 to 50 Hz, the modeled impedance curve is extrapolated to 3 Hz to show the sharp change in slope taking place at 5 Hz. The impedance curve presents a steep slope from 0 to 5 Hz which is a consequence of the structure behaving as a rigid body at low frequencies of excitation.

The modeled transmissibility curve, Figure 7.2, closely follows the 90% confidence interval reported by Pradko et al. (1967). The maximun reached by the model curve at 5 Hz exceeds the corresponding value on the upper limit of the experimental confidence interval by approximately 5.0%. The model transmissibility curve present a minimum at 14 Hz that deviates from the corresponding minimum on the lower boundary of the 90% confidence interval by approximately 18.0%. These are the two points showing the largest deviations from the experimental values. The reason for this behavior is most likely the fact that the upper torso being a deformable continuum has been modeled as a rigid mass. This will reduce the accuracy of the model predictions of intervertebral joint deformations at the lower end of the frequency interval 5-50 Hz.

From the results presented it is concluded that the response of the model is close enough to what can be expected from a subject seated in erect position and subjected to vertical sinusoidal oscillations. Therefore, the model will

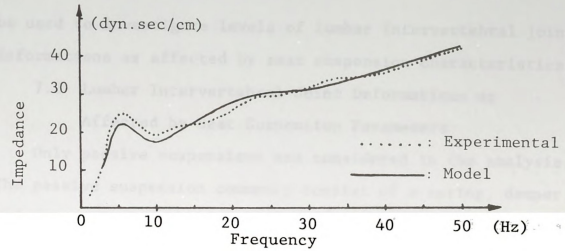

Figure 7.1. Driving point impedance for seated operator. Experimental curve from Pradko et al. (1967).

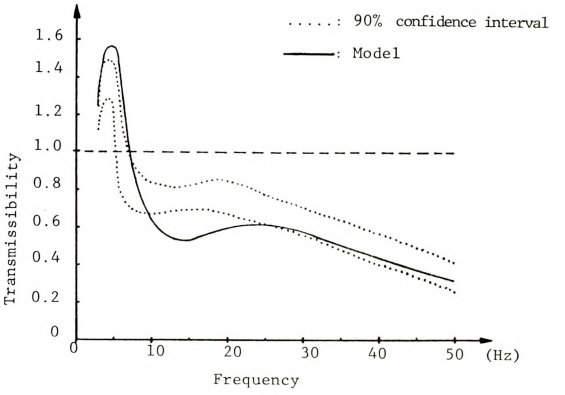

Figure 7.2. Seat to head transmissibility. Confidence interval from Pradko et al. (1967).

Experimental
0

be used to investigate levels of lumbar intervertebral joint deformations as affected by seat suspension characteristics.

7.2 Lumbar Intervertebral Joint Deformations as Affected by Seat Suspension Parameters

Only passive suspensions are considered in the analysis. The passive suspension commonly consist of a spring, damper, and mass. It is the simplest and most widely used for farm machinery. The mass associated with the suspension can be as low as 60.0 Kg (including the weight of the torso), for a suspended seat, and as high as 500.0 Kg for a suspended cab. The spring stiffness coefficient results from assuming a natural frequency for the suspended system between 2 and 4 Hz. The trend in the design of suspensions is toward lower natural frequencies in an attempt to reduce as much as possible the range of frequencies producing seat motion magnification, (seat displacement/chassis displacement >1.0). The limiting factor in the process of reducing natural frequency is the increasing static deflection permitted by the "soft" spring associated with low natural frequencies. The damping coefficient is set close to critical conditions to minimize oscillations for frequencies close to the natural frequency of the suspension.

The suspension parameters adopted for the analysis are given in Table 7.1.

An active suspension uses a power input to help minimize the motion of the seat under adverse terrain conditions, Roley and Burkhardt (1975).

Table 7.1. Seat and cab suspension parameters.

Type of suspension	K_c (dyn/cm) x 10^5	M_c (Kg)	C_c (dyn.sec/cm) x 10^5	C	ζ
seat	210.0	10.0	22.96	2.3	0.1
seat	210.0	10.0	22.96	15.0	0.65
seat	210.0	10.0	22.96	22.96	1.0
cab	1420.0	400.0	160.0	16.0	0.1
cab	1420.0	400.0	160.0	104.0	0.65
cab	1420.0	400.0	160.0	160.0	1.0

Natural frequency = 2.9 Hz

K_c : Suspension stiffness coefficient

M_c : Seat or cab mass

C : Suspension damping coefficient

C_c : Critical damping

ζ : Damping ratio = Actual damping/critical damping

Joint deformations are investigated for the three following conditions:

a) Subject sitting on a bare seat without suspension. The seat undergoes sinusoidal vertical motion

b) Subject sitting on a bare seat attached to the vibrating chassis through a spring-damper-mass suspension.

c) Subject sitting on a bare seat rigidly attached to a cab installed on a machine chassis through a spring-damper-mass suspension

7.2.1 Subject sitting on bare seat. No suspension

The lumbar intervertebral joints of a subject sitting on a bare rigid seat, subjected to vertical sinusoidal excitation are subjected to shear and axial deformations whose magnitudes are strongly dependent on the frequency of excitation, Figures 7.3 and 7.4. All deformations are given as percentage of chassis vertical amplitude of oscillation.

The maximum axial deformation takes place at the joint enclosed by the third and fourth lumbar vertebrae, level L3 - L4, while the maximum shear deformation takes place at the lumbo-sacral joint, level L5-S.

The axial deformation, Figure 7.3, sharply increases from 1.0 to 5.0% as frequencies changes from 3 to 5 Hz. No significant changes in axial deformations occur when varying frequency in the range 5 to 10 Hz. From 10 to 30 Hz deformation increases rapidly to reach a maximum of 20.0% of base amplitude between 35 and 45 Hz. Toward the end of the

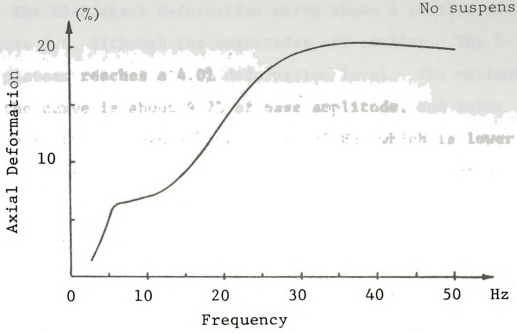

Figure 7.3. Axial deformation of L3 - L4 lumbar intervertebral joint.
(%): Percentage of base amplitude of motion

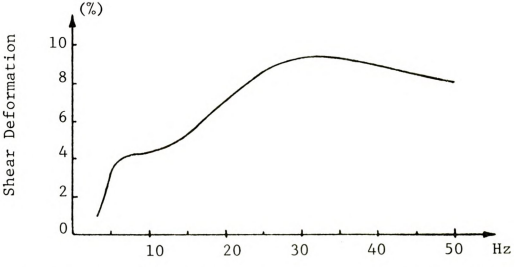

Figure 7.4. Shear deformation of L5 - S intervertebral joint.

frequency range studied the curve shows a decreasing trend.

The L5-S shear deformation curve shows a similar pattern, Figure 7.4, although the magnitudes are smaller. The 5-10 Hz plateau reaches a 4.0% deformation level. The maximum of the curve is about 9.2% of base amplitude, and takes place on the frequency range 30 to 35 Hz, which is lower than the range at which the axial deformations reach a maximum value.

The remaining lumbar intervertebral joints present significantly lower levels of deformation, but the shape of the curves is entirely similar; consequently only the numerical results are given in Appendices K to N.

7.2.2 Subject sitting on a bare seat provided with seat or cab suspension

The magnitude of joint deformations decreases significantly when the operator seat is attached to the vibrating chassis through a spring-damper-mass suspension. Figures 7.5 to 7.10 show deformation curves for suspended seat or cab, which reach much lower levels than those shown in Figures 7.3 and 7.4 for an operator sitting on a rigid table.

Three levels of suspension damping are anlyzed corresponding to 10, 65, and 100% of critical damping.

The magnitude of axial deformation at level L3-L4 are shown in Figure 7.5, for the cases of seat and cab suspensions under critical damping conditions. For most frequencies in the range 5-50 Hz the cab suspension results in lower joint deformations than the seat suspension. At 6 Hz the axial

deformations corresponding to the cab suspension curve exceed the deformations of the seat suspension curve by as much as 22%, but for all frequencies over 9 Hz the cab suspension offers better protection.

At 30 Hz the L3-L4 axial deformations corresponding to seat suspension exceed those of cab suspension by as much as 75%. A very similar situation takes place for shear deformations, as shown by Figure 7.6.

By decreasing the amount of damping the joint deformations are reduced for both seat and cab suspension as shown in Figures 7.7 and 7.8 which correspond to a damping coefficient equal to 65% of critical. The trend is larger deformation reductions at higher frequencies. For frequencies near the natural frequency of the suspension there is an increase of joint deformation, which can be clearly seen when the damping coefficient is further reduced.

By reducing the damping coefficient to only 10% of critical the deformations continue to decrease for frequencies over 10 Hz, but a resonant condition becomes evident at 3 Hz which is close to the natural frequency of the suspension system, Figures 7.9 and 7.10.

From the previous analysis it can be stated that a damper furnished with a variable damping coefficient can contribute to significant reductions of joint deformations. It should provide, for example, critical damping for frequencies close to the suspension natural frequency, but otherwise very light damping.

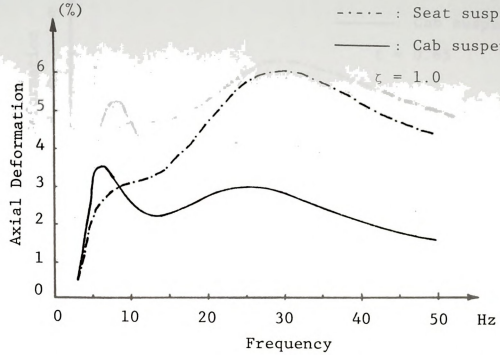

Figure 7.5. Axial deformations of L3 - L4 lumbar intervertebral joint.
(%): Percentage of base amplitude of motion

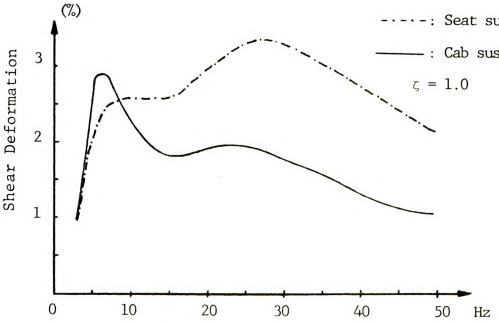

Figure 7.6. Shear deformations of L5 - S intervertebral joint.

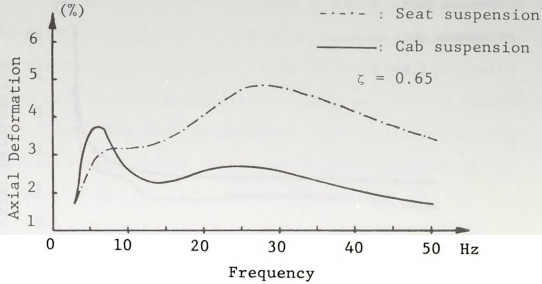

Figure 7.7. Axial deformation of L3 - L4 lumbar intervertebral joint.
(%): Percentage of base amplitude of motion

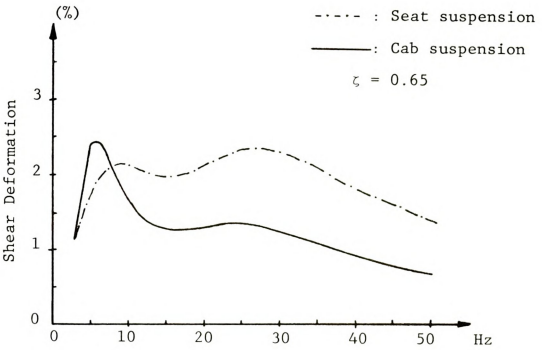

Figure 7.8. Shear deformation of L5 - S intervertebral joint.

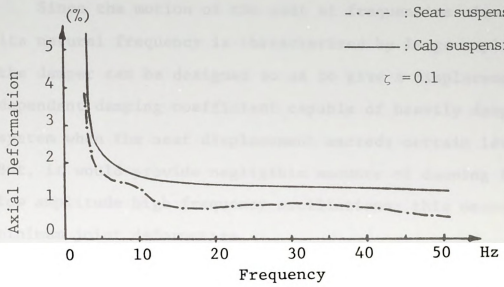

Figure 7.9. Axial deformation of L3 - L4 lumbar intervertebral joint.
(%): Percentage of base amplitude of motion

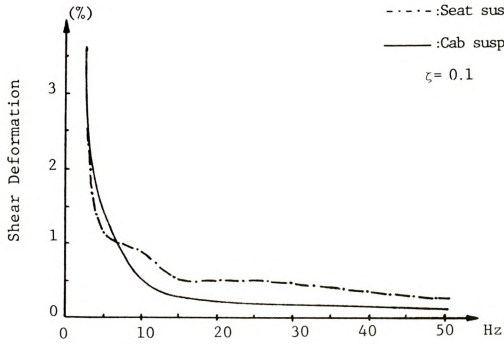

Figure 7.10. Shear deformation of L5 - S intervertebral joint.

Since the motion of the seat at frequencies close to its natural frequency is characterized by large amplitudes, the damper can be designed so as to give a displacement dependent damping coefficient capable of heavily damping the system when the seat displacement exceeds certain levels. But, it would provide negligible amounts of damping for low amplitude high frequency oscillations; this means minimum joint deformation.

7.3 Summary of Results

The main findings in this study are the following:

1. A lumped parameter model of the spine in the sagittal plane as the one shown in Figure 3.2 can closely predict the driving point impedance of an operator sitting in erect position while subjected to sinusoidal vertical oscillations.
2. The coefficient of transmissibility predicted by the model deviates as much as 18% from an experimentally determined 90% confidence interval reported in the literature. These deviations take place in the range 5 to 25 Hz. For higher frequencies the model predictions fall within the confidence interval.
3. Maximum axial intervertebral joint deformations take place at the joint located between the third and fourth lumbar vertebrae. The maximum shear deformation takes place at the lumbo-sacral intervertebral joint. These statements are valid over all the frequency range 5-50 Hz.

4. Frequencies over 15 Hz will sharply increase axial and shear joint deformations for a subject sitting on a bare vibrating seat. Axial deformation of joint L3 - L4 will almost triple when frequency is increased from 10 to 35 Hz. The shear deformation of joint L5 - S more than doubles for the same frequency increase.

5. The use of a spring-damper-mass suspension located between seat and chassis or between cab and chassis results in sharp reductions of joint deformations. The magnitude of the reduction depends on the type of suspension, the amount of damping, and the frequency of excitation.

6. Cab suspension can reduce joint deformation to almost half the levels corresponding to a seat suspension for frequencies over 10 Hz. Seat suspension can give joint deformations as much as 25% lower than cab suspension for frequencies between 5 and 10 Hz. Both types of suspensions were given identical damping ratios and natural frequency (2.9 Hz).

7. Low damping ratios ($\zeta = 0.1$) give the lowest joint deformations for most of the frequency range, but with very high values for frequencies near the natural frequency of the suspension system.

VIII. CONCLUSIONS AND RECOMMENDATIONS

8.1 Conclusions

The conclusions derived from this study are as follows:

1. The lumped parameter model developed in this investigation has shown promising results in predicting intervertebral joint deformations. It puts a word of warning on the well established criterion for design of seat suspension based mostly on comfort considerations.
2. The simplified substructure used to model the upper torso (single rigid mass) seems to be responsible for some discrepancies between the response of the model and the experimental data in the lower end of the frequency range 5-50 Hz.
3. When modeling the viscoelastic rheological behavior of intervertebral joints by means of Kelvin elements, the corresponding stiffness and damping coefficients vary exponentially with frequency.
4. The deformations of intervertebral joints are maximum for frequencies in the range 25 to 35 Hz. Since the rated speed of most engines used in modern farm equipment is between 1800 rpm (30 Hz) and 2600 rpm (40 Hz), the operator is exposed to vibrations in the most unfavorable range of frequencies from the stand point of joint deformations.

VIII. CONCLUSIONS AND RECOMMENDATIONS

8.1 Conclusions

5. Ride comfort has always been the criterion for the design of farm machinery seat suspension. This approach has led to the use of high values of damping in the process of minimizing the amplitude of motion at frequencies near the natural frequency of the seat. The result is a sharp increase of joint deformations for frequencies over 10 Hz that do not create immediate discomfort sensations but could be the reason for low back pain after years of exposure.

6. The joint deformations predicted by the model appear to be very small, but there are no data on what levels can be considered damaging under long time exposure conditions. The alternative left is to minimize deformations in order to offer maximum protection.
   The joint deformations reach at most a 20% of the amplitude of chassis oscillation which is already a small quantity for the case of vibrations generated as a result of minor unbalanced machine components having rotary or reciprocating motion.

7. The use of a spring-damper-mass suspension located between a seated operator and the vibrating chassis results in joint deformations about 1/4 to 1/5 of the values corresponding to a subject sitting on a seat rigidly attached to the chassis.

8. The use of cab suspension is desirable over seat suspension for the minimization of intervertebral joint deformations for frequencies over 10 Hz. Below 10 Hz the seat

suspension offers some advantage.

9. The use of a suspension damper capable of giving critical damping for excitation frequencies close to the natural frequency of the seat and very light damping for higher frequencies is desirable from the stand point of minimization of joint deformations.

8.2 Recommendations

Some of the changes that could be incorporated to the model to increase its range of applications and probably improve the occuracy of the results for the lower end of the frequency range 5-50 Hz are listed below:

1. The assumption made about small joint deformations must be relaxed if predictions of joint deformations are to be made in the range of low frequencies close to the natural frequency of the seat. It requires additional investigation of the kinematic and rheological behavior of the joints.

   By testing two consecutive vertebrae with the corresponding intervertebral joint, the patterns of relative motions could be studied.

   After motion and load histories have been recorded, the joint could be opened and all relevant dimensions taken for proper modeling of the kinematic behavior of the joint.

2. The seat to head transmissibility as well as the driving point impedance curves corresponding to a seated subject are quite sensitive to changes in bending stiffness and

damping coefficients. Therefore, more accurate data on bending rheological behavior of intervertebral joints is needed. Bending impedance tests of preloaded units similar to those carried out by Kazarian (1972), for axial motion, would be one approach to this problem.

3. If more accurate joint deformations are to be predicted for the thoracic spine, the ribcage requires a more elaborate model than a single mass suspended from the first 10 thoracic vertebrae. Ribs modeled as individual masses separated by viscoelastic elements representing the intercostal tissues, plus beam type elements representing the costo-vertebral and the costo-sternal joints would be an appropriate solution. The internal organs of the upper thorax could be modeled as rigid masses suspended from the ribcage by viscoelastic elements.

4. The joint deformations as presented in this report correspond to a point located in the center of the intervertebral disc at the intersection of the axis of the two vertebral bodies enclosing the disc. More severe deformations most likely occur at the articular facets on the posterior arch or at the opposite end of the joint on the annulus fibrosus.

   Some additional geometrical data plus some formulation could be added to the existing computer program to calculate those deformations.

REFERENCES

Andriacchi T., Schultz A., Belytschko T., and Galante J., 1974. A model for studies of mechanical interactions between the human spine and rib cage. Journal of Biomechanics 7: 497-507.

Baker L.D. and Wilkinson R.H., 1974. Occupational health survey of Michigan farmers. Department of Agricultural Engineering. Michigan State University, E. Lansing, Michigan. 88 p.

Beck J.V. and Arnold K.J., 1975. Parameter Estimation in Engineering and Science. Department of Mechanical Engineering, Michigan State University, E. Lansing, Michigan 48824.

Bell G.H., Olive and Beck J.S., 1967. Variations in strength of vertebrae with age and their relation to osteopososis. Calcified Tissue Research 1: 75-86.

Brown T., Hansen R.R., and Yorra A.J., 1957. Some mechanical tests on the lumbo-sacral spine with particular reference to the intervertebral discs. Journal of Bone and Joint Surgery 39A: 1135-1164.

Christ W. and Dupuis H., 1963. The influence of vertical vibrations on the spine and stomach. Translation No.153. Scientific Information Department. National Institute of Agricultural Engineering, Silsoe, England. 12 p.

Clark W.S., Lange K.O., and Coermann R.R., 1963. Deformation of the Human body due to uni-directional forced sinusoidal vibration pp 29-48, in S. Lippert, Ed., Human Vibration Research. Pergamon Ltd., Oxford, England. 111 p.

Clevenson A.S., and Leatherwood J.D., 1973. Development of Aircraft passenger Vibration Ride Acceptance Criteria. NASA Langley Research Center, Hampton, Virginia.

Coermann R.R., et al, 1960. The passive dynamic mechanical properties of the human thorax-abdomen system and the whole body system. Aerospace Medicine 31: 443-455.

Coermann R.R., 1963. The mechanical impedance of the human body in sitting and standing position at low frequencies. pp 1-28, in S. Lippert, Ed., Human Vibration Research. Pergamon Press Ltd., Oxford, England 111 p.

Crocker J.F., Higgins L.S., 1966. Phase IV - Investigation of strenth

of isolated vertebrae. Final report NASA contract No. NASW-1313. Technology Inc., San Antonio, Texas.

Damon A., Stoudt H. and McFarland R.R., 1966. The Human Body in Equipment Design. Harvard University Press. Massachusetts. 355 p.

Dempster W.T., 1955. Space requirements of the seated operator. Wright Air Development Center Technical Report 55-159, Project No.7214. Wright-Patterson Air Force Base, Ohio.

Eie N., 1972. Recent measurements of the intra-abdominal pressure. pp 121-122, in R.M. Kenedi, Ed., Perspectives in Biomedical Engineering. Pergamon Press Ltd., Oxford, England.

Evans G.F. and Lissner H.R., 1959. Biomechanical studies on the lumbar spine and pelvis. Journal of Bone and Joint Surgery 41-A: 278-290.

Ewing C.L., King A., and Prasad P., 1972. Structural considerations of the human vertebral column under + Gz impact acceleration. Journal of Aircraft 9: 84-90.

Foss K.A., 1958. Coordinates which uncouple the equations of motion of damped linear dynamic systems. Journal of Applied Mechanics 25: 361-364.

Fusco M., et al., 1963. Effect of vibration on the peripheral vascular system and on the vertebral column. Folia Medica 46: 361-372.

Gere, J.M. and Weaver W. Jr., 1965. Analysis of Framed Structures. Van Nostrand Reinhold Company, New York. 475 pp.

Gruber G.J., and Ziperman H.H., 1974. Relationship between whole-body vibration and morbidity patterns among motor coach operators Publication No.(NIOSH) 75-104. National Institute for Occupational Safety and Health. Cincinnati, Ohio.

Hopkins G.R., 1970. Nonlinear lumped parameter mathematical model of dynamic response of the human body. Symposium on Biodynamic Models and their Applications, AMRL-TR-71-29. Wright Petterson Air Force Base, Ohio.

Hornick R., 1961. Effects of tractor vibration on operators. Agricultural Engineering 42: 674-675, 696-697.

Ingalls N.W., 1931. Observations on bone weights. American Journal of Anatomy 48: 48-98.

Kazarian L., 1972. Dynamic response characteristics of the human vertebral column. Acta Orthopedica Scandinavica 146: 186 p.

King A.I., and Vulcan A.P., 1971. Elastic deformation characteristics of the spine. Journal of Biomechanics 4: 413-429.

Kraus H., and Farfan H., 1972. Stress analysis of human intervertebral disc. Proceeding of the 25 th. Annual Conference on Engineering in Medicine and Biology.

Lanier R., 1939. The presacral vertebrae of american white and negro males. American Journal of Physical Anthropology 25: 341-420.

Liu Y.K., Laborde J.M., and Van Buskirk M.C., 1971. Inertial properties of a segmented cadaver trunk: their implications in acceleration injures. Aerospace Medicine 42: 650-657.

Liu Y.K., and Wickstrom J.K., 1973. Estimation of the inertial property distribution of the human torso from segmented cadaver data. pp 203-213, in R.M., Kenedi, Ed., Prospectives in Biomedical Engineering. University Park Press, Baltimore.

Lowrance E.W., and Latimer H.B., 1967. Weights and variability of components of the human vertebral column. Anatomical Record 159: 83-88.

Markolf K., and Steidel R., 1970. The dynamic characteristics of the human intervertebral joint. American Society of Mechanical Engineering, paper 70WA/BHF6. 11 p.

Martin G.H., 1969. Kinematics and Dynamics of Machines. McGraw-Hill, Inc., New York. 495 p.

Martin H.C., 1966. Introduction to Matrix Methods of Structural Analysis McGraw-Hill Book Company, New York. 331 p.

Meirovitch L., 1967. Analytical Methods in Vibrations. The MacMillan Co., N. York, N.Y. 10022.

Miksian R., 1970. A non-linear model of the human body in the sitting position subjected to sinusoidal displacements of the seat. Ph.D. Thesis, Department of Mechanical Engineering and Applied Mechanics, University of Rhode Island, Kingston Rhode Island.

Miksian R., and Nash C.D. Jr., 1974. A model for the response of seated humans to sinusoidal displacement of the seat. Journal of Biomechanics 7: 209-215.

Orne D., and King Liu Y., 1971. A mathematical model of spinal response to impact. Journal of Biomechanics 4: 49-71.

Paulson E.C., 1949. Tractor driver's complaints. Minnesota Medicine 32: 386-387.

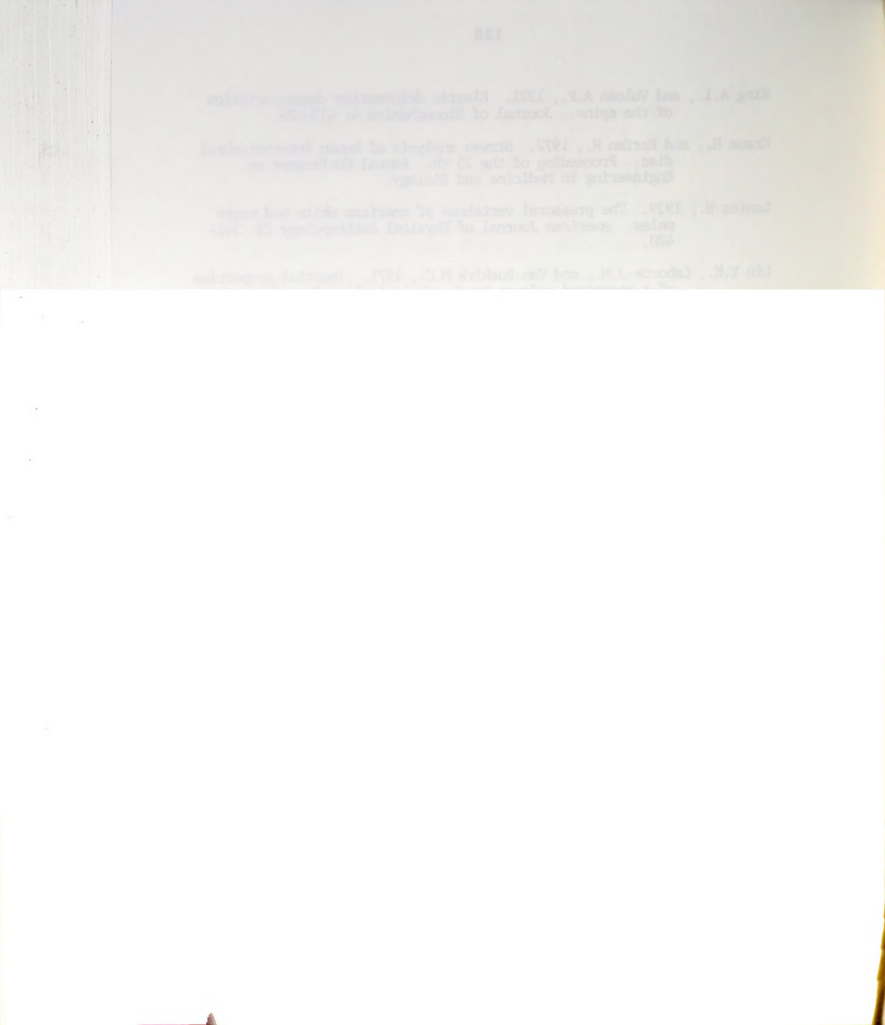

Payne P.R. and Band E.G.U., 1969. A four degree of freedom lumped parameter model of the seated human body. Paper No.59101-6. Wyle Laboratories, Payne Division, Rockville, Maryland 20852.

Payne P.R., 1970. Some aspects of biodynamic modeling for aircraft escape systems. pp 233-335. Symposium on Biodynamic Models and their Applications, AMRL-TR-71-29. Wright-Patterson Air Force Base, Ohio.

Pradko F., Lee R.A., and Greene J.D., 1967. Human vibration response theory. pp 205-222. Biomechanics Monographs. American Society of Mechanical Engineers. 245 p.

Prasad P., and King A.I., 1974. An experimentally validated dynamic model of the spine. Journal of Applied Mechanics 41: 546-550.

Prives M.G., 1960. Influence of labor and sports upon skeleton structure in man. Anatomical Record 136: 261-271.

Reismann H. and Pawlik P.S., 1975. Elastokinetics - An Introduction to the Dynamics of Elastic System. West Publishing Co., St. Paul Minnesota.

Roberts S.B., and Chen P.H., 1970. Elastostatic analysis of the human thoracic skeleton. Journal of Biomechanics 3: 527-546.

Roley D.G., and Burhardt T.H., 1975. Performance characteristics of cab suspension models. American Society of Agricultural Engineers. Paper No.75-1517. St. Joseph, Michigan 49085. 15 p.

Rosegger R., and Rosegger S., 1960. Health effects of tractor driving. Journal of Agricultural Engineering Research 5: 241-275.

Sandover J., 1970. Some current biomechanical research in the United Kingdom. pp 105 - 122. Symposium on Biodynamic Models and their Applications, AMRL-TR-71-29. Wright-Patterson Air Force Base, Ohio 45433.

Schultz, A.B., and Galante J.O., 1970. A mathematical model for the study of the mechanics of the human vertebral column. Journal of Biomechanics 3: 405-416.

Schultz A.B., Belytschko T.B., and Andriacchi T.P., 1973. Analog studies of forces in the human spine: mechanical properties and motion segment behavior. Journal of Biomechanics 6: 373-383.

Schultz A.B., Benson D.R., and Hirsch C., 1974. Force-deformation properties of human costo-sternal and costo-vertebral articulations. Journal of Biomechanics 7: 311-318.

Suggs C.W., Abrams C.F., and Stikeleather L.F., 1969. Application of a damped spring-mass human vibration simulator in vibration testing of vehicle seats. Ergonomics 12: 79-90.

Thomson W.T., 1972. Theory of Vibrations With Applications. Prentice-Hall, Inc. Englewood Cliffs, New Jersey.

Vernon J.B., 1967. Linear Vibration Theory. Wiley Inc., New York. 364 p.

Vulcan A.P. and King A.I., 1971. Forces and moments sustained by the lower vertebral column of a seated human during seat-to head acceleration. pp 84 - 99. Dynamic Response of Biomechanical Systems, The American Society of Mechanical Engineers. New York.

Wasserman D.E., Badger D.W., Doyle T.E., and Margolies L., 1974. Industrial vibrations - an overviwe. American Society of Safety Engineers Journal, June: 35 - 43.

Weis E.B., Clarke N.P., and vonGierke H.E., 1966. Mechanical Impedance as a tool in biomechanics. Paper No. AMRL-TR-66-84, pp 23. Aeromedical Research Laboratories, Wright Patterson Air Force Base, Ohio.

Yeager R.R., Machowsky G.V., and Shanahan R.J., 1969. Development of a dynamic model of unrestrained seated man subjected to impact. Paper No.NADC-AC-6902. Technology Inc., San Antonio, Texas.

APPENDICES

APPENDIX A

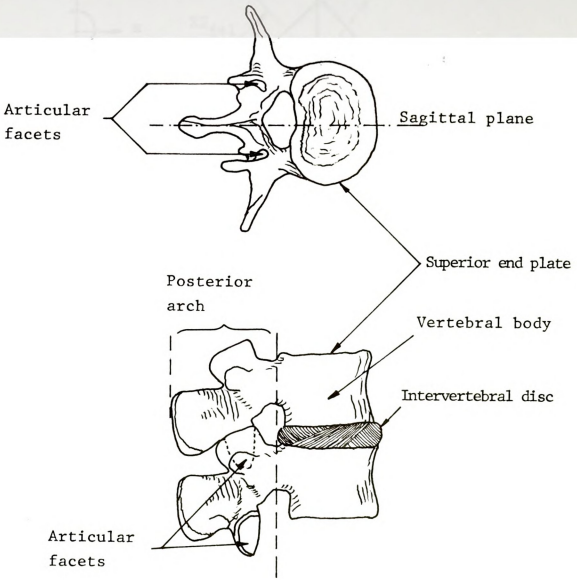

Figure A.1. Main structural components of vertebral column

APPENDIX B

Governing Equation Describing the Motion of a Vertebra in x-direction

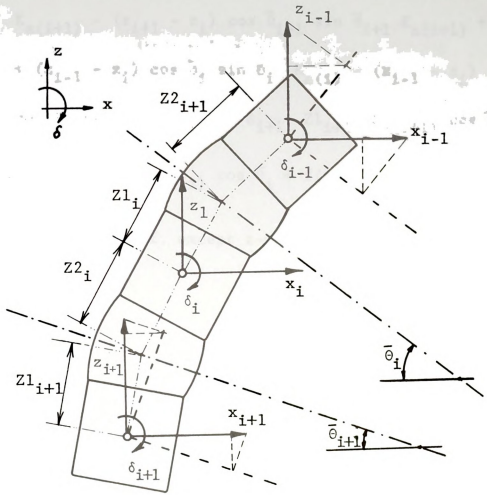

Figure B.1. Displacements affecting the equilibrium of vertebral mass m_i in x-direction.

From Newton's 2nd. law: $m \ddot{x}_i$ = (Forces acting on m_i in direction)

$$m \ddot{x}_i = (x_{i+1} - x_i) \cos^2 \bar{\theta}_{i+1} \; K_{s(i+1)} + (x_{i+1} - x_i) \sin^2 \bar{\theta}_{i+1}$$

$$K_{a(i+1)} + (x_{i-1} - x_i) \cos^2 \bar{\theta}_i \; K_{s(i)} + (x_{i-1} - x_i)$$

$$\sin^2 \bar{\theta}_i \; K_{a(i)} + (z_{i+1} - z_i) \cos \bar{\theta}_{i+1} \; \sin \bar{\theta}_{i+1}$$

$$K_{a(i+1)} - (z_{i+1} - z_i) \cos \bar{\theta}_{i+1} \sin \bar{\theta}_{i+1} \; K_{s(i+1)} +$$

$$+ (z_{i-1} - z_i) \cos \bar{\theta}_i \sin \theta_i \; K_{a(i)} - (z_{i-1} - z_i)$$

$$\cos \theta_i \sin \bar{\theta}_i \; K_{s(i)} + \delta_{i+1} \; Z1_{i+1} \; K_{s(i+1)} \cos \bar{\theta}_{i+1} -$$

$$- \delta_{i-1} \; Z2_{i-1} \; K_{s(i)} \cos \bar{\theta}_i + f(t)$$

$f(t) = 0$ for all d.f. except z-motion of sacrum-pelvis mass.

APPENDIX C

Table C.1. Distribution of degrees of freedom corresponding to each rigid moving component of the model.

Element	Motion	Degree of freedom number
Head-neck	x	1
Head neck	z	2
Head-neck	δ	3
Th1	x	4
Th1	z	5
Th1	δ	6
Th2	x	7
.	.	.
.	.	.
.	.	.
Th12	S	39
L1	x	40
L1	z	41
L1	δ	42
.	.	.
.	.	.
.	.	.
.	.	.
L5	x	52
L5	z	53
L5	δ	54
Sacrum-Pelvis	x	55
Sacrum-Pelvis	z	56
Thorax	x	57
Thorax	z	58

APPENDIX D

Stiffness Matrix Corresponding to an Intervertebral Joint

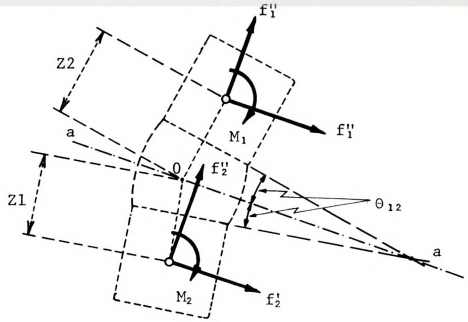

Figure D.1. Forces acting on an intervertebral joint

The joint stiffness matrix can be obtained by applying the definition given by Vernon (1967): " k_{ij} is the load required in the direction of coordinate i when a unit displacement occurs in the direction of coordinate j and all other displacements are zero". So a unit displacement will be given to one coordinate at a time of the system in Figure D.1, and forces in all six directions calculated from the equations of static equilibrium.

The equation of static equilibrium of an intervertebral

joint are as given by equations D-1 to D-3.

$$\Sigma F_u = f_1' + f_2' = 0 \quad ; \quad f_2' = - f_1' \tag{D.1}$$

$$\Sigma F_w = f_1'' + f_2'' = 0 \quad ; \quad f_2'' = - f_1'' \tag{D.2}$$

$$\Sigma M_0 = M_1 + M_2 - f_1' \; Z2 \; \cos \theta_{12} - f_2' \; Z1 \cos \theta_{12} +$$

$$+ f_1'' \; Z2 \sin \theta_{12} - f_2'' \; Z1 \sin \theta_{12} = 0 \tag{D.3}$$

Calculation of stiffness coefficients k_{j1}:

A unit displacement of the superior vertebra in u-direction, while the inferior vertebra is maintained fixed, develops a reaction at the intervertebral joint as shown in Figure D.2 (a).

$u_1 = 1 \; ; \; k_{11} = f_1' \; ; k_{21} = f_1'' \; ; \; k_{31} = M_1$

$k_{41} = f_2' \; ; \; k_{51} = f_2'' \; ; \; k_{61} = M_2$

$\Sigma F_u = f_1' - k_s = 0 \qquad f_1' = \underline{k_{11} = K_s}$

$\Sigma F_w = 0$ no forces in w - directions $\qquad f_1'' = \underline{k_{21} = 0}$

$\Sigma M_0 = M_1 - f_1' \times Z2 \; \cos \theta_{12} = 0 \quad M_1 = \underline{K_{31} = K_s Z2 \cos \theta_{12}}$

From equations (D.1) to (D.3):

$f_2' = - f_1' = - K_s$ $\qquad$ $\underline{k_{41} = - K_s}$

$f_2'' = - f_1'' = 0$ $\qquad$ $\underline{k_{51} = 0}$

$M_2 = - K_s \, Z1 \cos$ $\qquad$ $\underline{k_{61} = - K_s \, Z1 \cos \theta_{12}}$

Calculation of coefficients k_{j2}:

A unit displacement of the superior vertebra in w-direction, while the inferior vertebra is maintained fixed, develops a reaction at the intervertebral joint as shown in Figure D.2 (b).

$w_1 = 1$ $\qquad$ $k_{12} = f_1'$ $\qquad$ $k_{22} = f_1''$ $\qquad$ $k_{32} = M_1$

$k_{42} = f_2'$ $\qquad$ $k_{52} = f_2''$ $\qquad$ $k_{62} = M_2$

$\Sigma F_u = 0$ no forces in u-direction $\qquad f_1' = \underline{k_{12} = 0}$

$\Sigma F_w = f_1'' - K_a = 0$ $\qquad f_1'' = \underline{k_{22} = K_a}$

$\Sigma M_0 = M_1 + f_1'' \, Z2 \sin \theta_{12} = 0$ $\qquad M_1 = \underline{k_{32} = -K_a Z2 \sin \theta_{12}}$

From equations (D.1) to (D.3):

$f_2' = - f_1' = 0$ $\qquad$ $\underline{k_{42} = 0}$

$f_2'' = - f_1'' = -K_a$ $\qquad k_{52} = - K_a$

$M_2 = - K_a Z1 \sin \theta_{12}$ $\qquad k_{62} = - K_a Z1 \sin \theta_{12}$

Calculation of coefficients k_{j3}:

A unit rotation of the superior vertebra, while the inferior is maintained fixed, develops the reactions shown in Figure D.2(c) at the intervertebral joint.

$\delta_1 = 1$ $\quad k_{13} = f_1'$ $\quad k_{23} = f_1''$ $\quad k_{33} = M_1$

$k_{43} = f_2'$ $\quad k_{53} = f_2''$ $\quad k_{63} = M_2$

$\Sigma F_u = f_1' - K_s Z2 \cos\theta_{12} = 0$ $\qquad f_1' = k_{13} = K_s Z2 \cos \theta_{12}$

$\Sigma F_w = f_1'' + K_a Z2 \sin\theta_{12} = 0$ $\qquad f_1' = k_{23} = - K_a Z2 \sin \theta_{12}$

$\Sigma M_0 = M_1 - K_b + Z2 (f_1'' \sin \theta_{12} - f_1' \cos\theta_{12})$. $M_1 = k_{33} = K_b + Z2^2 (K_s \cos^2\theta_{12} + K_a \sin^2 \theta_{12})$

From equations (D.1) to (D.3):

$f_2' = - f_1'$ $\qquad f_2' = k_{43} = - K_s Z2 \cos \theta_{12}$

$f_2'' = - f_1''$ $\qquad f_2'' = k_{53} = K_a Z2 \sin \theta_{12}$

$M_2 = k_{63} = - K_b + Z1 Z2 (K_a \sin^2\theta_{12} - K_s \cos^2 \theta_{12})$

Calculation of coefficients k_j4:

Similar procedure is followed when giving unit displacements to the inferior vertebra. Only the equations are shown below.

$u^2 = 1$ (Figure D.2 (d))

$k_{14} = f_1'$ $\quad k_{24} = f_1''$ $\quad k_{34} = M_1$

$k_{44} = f_2'$ $\quad k_{54} = f_2'$ $\quad k_{64} = M_2$

$\Sigma F_u = 0$ $\quad f_2' = \underline{k_{44} = K_s}$

$\Sigma F_w = 0$ $\quad f_2'' = \underline{k_{54} = 0}$

$\Sigma M_0 = 0$ $\quad M_2 = \underline{k_{64} = K_s Z1 \cos \theta_{12}}$

From equations (D.1) to (D.3):

$f_1' = - f_2'$ $\quad f_1' = \underline{k_{14} = - K_s}$

$f_1'' = - f_2''$ $\quad f_1'' = \underline{k_{24} = 0}$

$M_1 = - M_2 + (f_1' Z2 + f_2' Z1) \cos \theta_{12} - (f_1'' Z2 - f_2'' Z1) \sin \theta_{12}$

$M_1 = \underline{k_{34} = - K_s Z2 \cos \theta_{12}}$

Calculation of coefficients k_{j5}:

$w_2 = 1$ (Figure D.2 (e))

$k_{15} = f_1'$ $\quad k_{25} = f_1''$ $\quad k_{35} = M_1$

$k_{45} = f_2'$ $\quad k_{55} = f_2''$ $\quad k_{65} = M_2$

$\Sigma F_u = 0 \qquad f_2' = \underline{k_{45} = 0}$

$\Sigma F_w = 0 \qquad f_2'' = \underline{k_{55} = K_a}$

$\Sigma M_0 = 0 \qquad M_2 = \underline{f_2'' \; Z1 \sin \theta_{12}}$

From equations (D.1) to (D.3):

$f_1' = - f_2' \qquad f_1' = \underline{k_{15} = 0}$

$f_1'' = - f_2'' \qquad f_1'' = \underline{k_{25} = - K_a}$

$M_1 = -M_2 + (f_1' \; Z2 + f_2' \; Z1) \cos \theta_{12} - (f_1'' \; Z2 - f_2'' \; Z1) \sin \theta_{12}$

$M_1 = \underline{k_{35} = K_a \; Z2 \sin \theta_{12}}$

Calculation of coefficients k_{j6}:

$\delta_2 = 1$ (Figure D.2 (f))

$k_{16} = f_1'$ $\quad k_{26} = f_1''$ $\quad k_{36} = M_1$

$k_{46} = f_2'$ $\quad k_{56} = f_2''$ $\quad k_{66} = M_2$

$\Sigma F_u = 0 \qquad f_2' = \underline{k_{46} = K_s \, Z1 \cos \theta_{12}}$

$\Sigma F_w = 0 \qquad f_2'' = \underline{k_{56} = K_a \, Z1 \sin \theta_{12}}$

$\Sigma M_0 = 0 \qquad M_2 = k_{66} = \underline{K_b + Z1^2 \left(K_s \cos^2 \theta_{12} + K_a \sin^2 \theta_{12} \right)}$

From equations (D.1) to (D.3):

$f_1' = - f_2' \qquad f_1' = \underline{k_{16} = - K_s \, Z1 \cos \theta_{12}}$

$f_1'' = - f_2'' \qquad f_1'' = \underline{k_{26} = - K_a \, Z1 \sin \theta_{12}}$

$M_1 = \underline{k_{36} = - K_b + Z1 \, Z2 \, (K_a \sin^2 \theta_{12} - K_s \cos^2 \theta_{12})}$

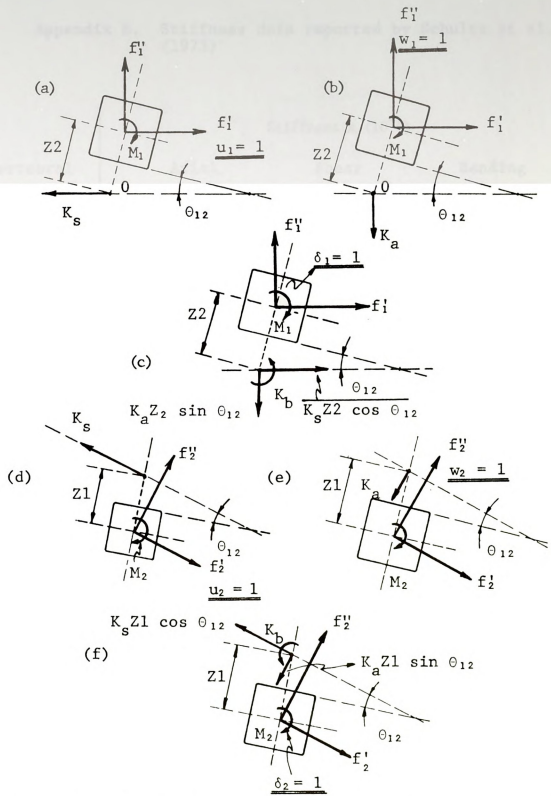

Figure D.2. Forces developed at the intervertebral joint as a result of unit displacements of the adjacent vertebra.

Appendix E. Stiffness data reported by Schultz et al. (1973)

Vertebral level	Stiffness x (10^{-5}) Axial dyn/cm	Shear dyn/cm	Bending dyn.cm/rad.
T1	6863.1	5882.6	1960.9
T2	11765.3	10784.8	3921.7
T3	14706.6	13726.1	5882.6
T4	20589.2	18628.4	9804.4
T5	18628.3	16667.5	9804.4
T6	17647.9	15687.0	9804.4
T7	14706.6	13726.1	9804.4
T8	14706.6	12745.7	10784.8
T9	14706.6	13726.1	10784.8
T10	14706.6	13726.1	11765.3
T11	14706.6	10784.8	9804.4
T12	17647.9	9804.4	8823.9
L1	15687.0	8823.9	8823.9
L2	14706.6	7843.5	8823.9
L3	14706.6	7843.5	8823.9
L4	13726.16	6863.1	7843.5
L5	10784.8	5882.6	6863.1

APPENDIX F

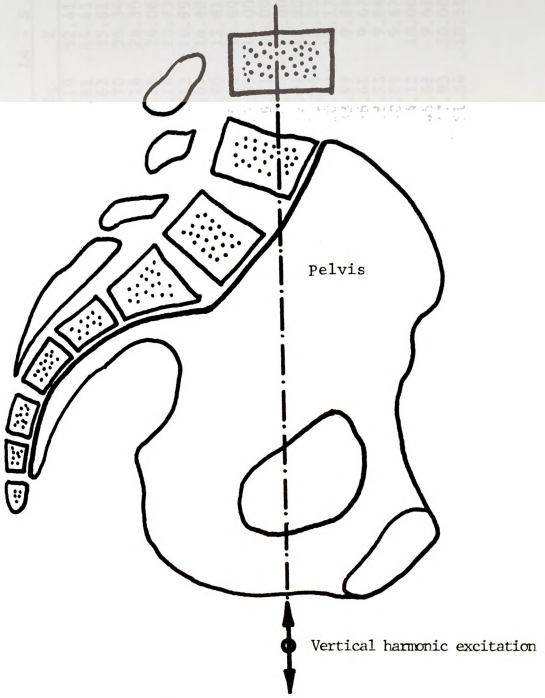

Figure F.1. Vertical excitation of the spine through the pelvis.

APPENDIX G

Table G.1. Experimental mechanical impedance. Age: less than 30, Kazarian (1972).

T1 - T6			T7 - T12			L1 - L3			L4 - S		
fq	Z	Ψ	fq	Z	Ψ	fq	Z	Ψ	fq	Z	Ψ
5.04	74.06	81.0	5.03	108.57	82.0	5.03	76.86	82.0	5.10	52.41	82.0
5.56	71.63	81.0	5.58	101.66	82.0	5.58	71.97	82.0	5.61	44.41	82.0
6.04	68.13	81.0	6.01	93.63	82.0	5.97	68.50	82.0	6.62	35.81	82.0
6.60	63.73	81.0	6.58	87.67	82.0	6.53	63.10	82.0	7.70	30.34	82.0
7.03	61.64	81.0	7.04	83.45	82.0	6.99	58.11	82.0	8.14	28.39	82.0
7.38	64.80	81.0	7.54	79.43	82.0	7.49	54.41	82.0	9.15	24.06	82.0
8.07	60.62	81.0	8.03	76.86	82.0	8.03	52.65	82.0	10.14	20.73	82.0
8.59	57.66	81.0	8.54	71.97	82.0	8.54	51.79	82.0	12.12	16.99	82.0
9.08	53.04	81.0	9.02	68.50	82.0	8.96	51.79	82.0	13.07	14.88	82.0
10.07	47.20	81.0	9.34	67.39	82.0	9.66	50.12	82.0	14.90	12.61	82.0
11.09	44.15	81.0	10.00	60.06	82.0	10.14	44.67	82.0	16.18	11.80	82.0
11.97	42.70	81.0	10.86	50.12	82.0	11.40	27.72	82.0	17.33	12.00	82.0
13.56	39.28	81.0	12.21	37.28	82.0	12.12	25.96	82.0	19.21	12.00	82.0
14.73	36.75	81.0	14.10	29.61	82.0	13.72	25.96	82.0	20.44	12.00	82.0
16.91	34.37	81.0	16.18	24.31	82.0	16.07	23.91	82.0	22.97	11.80	82.0
20.38	31.62	81.0	20.16	24.71	82.0	18.06	26.83	82.0	26.54	12.20	82.0
23.57	30.58	81.0	21.89	23.14	82.0	20.30	31.62	82.0	30.87	10.17	82.0
26.88	29.09	81.0	24.27	19.95	82.0	23.61	27.27	82.0	33.99	9.84	82.0
30.87	26.32	81.0	27.85	15.59	82.0	27.09	24.71	82.0	36.41	9.67	82.0
33.54	24.21	81.0	30.45	12.18	82.0	30.45	22.76	82.0	38.73	9.84	82.0
37.72	22.28	81.0	32.84	11.04	82.0	33.99	20.28	82.0	40.09	9.67	82.0
41.27	21.54	81.0	36.66	10.00	82.0	38.47	17.49	82.0	44.13	10.00	82.0
45.46	20.84	81.0	39.54	8.21	82.0	40.64	16.11	82.0	45.68	9.67	82.0
51.13	20.15	81.0	44.13	7.81	82.0	45.05	14.84	82.0	47.93	10.00	82.0
			50.64	9.84	82.0	50.64	13.45	82.0	51.34	10.51	82.0

fq (Hz); Z (lb.sec/in); Ψ (deg)

Table G.2. Experimental mechanical impedance. Age 30 to 50, Kazarian (1972).

T1 - T6			T7 - T12			L1 - L3			L4 - S		
fq	Z	Ψ	fq	Z	Ψ	fq	Z	Ψ	fq	Z	Ψ
4.98	101.67	81.0	5.03	84.83	82.0	5.01	95.19	82.0	5.11	84.83	82.0
5.53	103.37	81.0	5.58	84.83	82.0	5.51	92.11	82.0	5.66	76.86	82.0
6.00	100.00	81.0	6.01	84.83	82.0	5.94	89.13	82.0	6.11	74.38	82.0
6.52	95.15	81.0	6.58	86.24	82.0	6.94	84.83	82.0	6.58	71.97	82.0
7.04	93.59	81.0	7.04	89.13	82.0	6.95	82.09	82.0	7.10	68.50	82.0
7.59	90.54	81.0	7.54	89.13	82.0	7.92	80.75	82.0	7.65	65.21	82.0
8.53	84.73	81.0	8.03	87.67	82.0	8.60	78.14	82.0	8.09	62.07	82.0
9.53	83.34	81.0	8.60	84.83	82.0	9.86	69.64	82.0	9.09	58.11	82.0
10.00	83.34	81.0	9.02	83.45	82.0	10.71	62.07	82.0	10.07	56.23	82.0
10.57	84.73	81.0	9.53	80.75	82.0	12.12	54.41	82.0	10.71	44.67	82.0
11.56	76.72	81.0	10.00	78.14	82.0	13.43	48.50	82.0	12.20	37.28	82.0
13.92	70.62	81.0	11.47	71.97	82.0	15.94	44.67	82.0	14.18	34.90	82.0
16.31	66.09	81.0	12.21	66.29	82.0	17.18	47.71	82.0	16.27	34.33	82.0
18.60	60.84	81.0	14.20	59.08	82.0	19.31	48.50	82.0	18.28	32.15	82.0
20.20	58.86	81.0	16.74	48.50	82.0	21.84	39.16	82.0	20.26	31.11	82.0
21.49	57.89	81.0	20.16	39.81	82.0	23.71	34.33	82.0	23.55	28.18	82.0
24.50	55.08	81.0	22.81	34.90	82.0	26.10	34.33	82.0	26.46	25.54	82.0
28.32	49.05	81.0	26.54	30.10	82.0	27.76	35.48	82.0	30.56	21.31	82.0
30.55	49.05	81.0	30.45	29.61	82.0	30.14	32.68	82.0	33.87	19.95	82.0
32.96	45.91	81.0	36.66	29.61	82.0	33.18	30.10	82.0	37.79	18.68	82.0
36.80	40.88	81.0	40.64	30.10	82.0	37.02	28.65	82.0	41.03	17.49	82.0
40.81	35.81	81.0	45.05	29.13	82.0	40.19	27.72	82.0	44.24	16.65	82.0
44.95	37.01	81.0	50.29	28.65	82.0	44.55	25.12	82.0	47.06	16.93	82.0
50.88	41.56	81.0				50.05	23.52	82.0	50.74	17.78	82.0

fq: frequency (Hz); Z: impedance (lb.sec/in); Ψ: phase angle (deg)

Table G.3. Experimental mechanical impedance. Age: over 50, Kazarian (1972).

T1 - T6			T7 - T12			L1 - L3			L4 - S		
fq	Z	Ψ	fq	Z	Ψ	fq	Z	Ψ	fq	Z	Ψ
5.04	81.97	81.0	5.04	95.19	82.0	4.97	117.88	82.0	5.13	65.21	82.0
5.59	83.34	81.0	5.98	98.37	82.0	5.55	114.06	82.0	6.14	55.32	82.0
6.04	81.97	81.0	6.49	98.37	82.0	5.94	112.20	82.0	7.14	45.41	82.0
6.65	78.00	81.0	7.00	98.37	82.0	6.49	106.80	82.0	7.70	42.52	82.0
7.08	76.72	81.0	7.50	96.76	82.0	6.95	103.34	82.0	8.14	39.81	82.0
7.64	74.22	81.0	8.90	92.11	82.0	7.45	98.37	82.0	8.66	37.89	82.0
8.07	73.00	81.0	9.47	92.11	82.0	8.48	92.11	82.0	9.15	35.48	82.0
8.65	71.00	81.0	11.87	79.43	82.0	9.40	86.24	82.0	10.21	31.11	82.0
9.08	70.62	81.0	13.89	70.79	82.0	10.28	78.14	82.0	12.29	25.12	82.0
9.59	69.46	81.0	14.58	70.79	82.0	11.95	46.93	82.0	14.59	21.66	82.0
10.14	69.46	81.0	16.72	59.08	82.0	13.06	41.82	82.0	16.29	19.95	82.0
11.48	69.46	81.0	17.91	57.17	82.0	14.18	39.81	82.0	18.18	21.31	82.0
15.89	74.22	81.0	20.12	47.71	82.0	15.51	37.28	82.0	20.30	22.39	82.0
20.38	73.00	81.0	22.14	45.41	82.0	16.27	35.48	82.0	22.66	20.96	82.0
23.90	68.32	81.0	23.71	43.94	82.0	18.28	36.67	82.0	25.29	19.63	82.0
28.21	63.94	81.0	25.75	39.16	82.0	20.12	38.52	82.0	26.36	20.28	82.0
30.87	61.85	81.0	27.76	39.81	82.0	22.91	41.82	82.0	27.09	19.63	82.0
34.72	58.86	81.0	30.14	39.81	82.0	26.64	41.82	82.0	28.04	17.78	82.0
37.98	54.18	81.0	32.50	38.52	82.0	30.14	41.82	82.0	30.87	16.38	82.0
41.27	52.41	81.0	36.27	39.16	82.0	35.29	42.52	82.0	35.42	13.89	82.0
45.15	50.70	81.0	40.19	41.14	82.0	36.27	41.82	82.0	39.27	12.59	82.0
48.38	49.87	81.0	44.24	41.14	82.0	39.92	32.15	82.0	41.20	12.38	82.0
51.49	49.87	81.0	46.42	39.81	82.0	44.85	32.15	82.0	45.68	13.01	82.0
			50.05	40.47	82.0	50.05	32.15	82.0	51.34	14.84	82.0

fq: frequency H ; Z: Mechanical impedance (lb.sec/in); Ψ: phase angle (deg)

APPENDIX H

Table H.1. Transmissibility data, Pradko (1967)

Frequency	Mean	Standard Deviation	Confidence Interval (90%)	
			Upper Bound	Lower Bound
1	1.011	.032	1.032	.989
3	1.182	.105	1.253	1.111
4	1.389	.157	1.495	1.282
5	1.298	.302	1.401	1.195
7	.901	.282	1.092	.710
10	.76	.20	.836	.684
15	.74	.23	.828	.652
20	.76	.22	.843	.677
30	.63	.18	.698	.562
40	.49	.14	.570	.410
50	.35	.12	.423	.277
60	.25	.12	.302	.198